

This work was written as part of one of the author's official duties as an Employee of the United States Government and is therefore a work of the United States Government. In accordance with 17 U.S.C. 105, no copyright protection is available for such works under U.S. Law.

Public Domain Mark 1.0

<https://creativecommons.org/publicdomain/mark/1.0/>

Access to this work was provided by the University of Maryland, Baltimore County (UMBC) ScholarWorks@UMBC digital repository on the Maryland Shared Open Access (MD-SOAR) platform.

**Please provide feedback**

Please support the ScholarWorks@UMBC repository by emailing [scholarworks-group@umbc.edu](mailto:scholarworks-group@umbc.edu) and telling us what having access to this work means to you and why it's important to you. Thank you.

# ISS as a Platform for Optical Remote Sensing of Ecosystem Carbon Fluxes: A Case Study Using HICO

Karl Fred Huemmrich<sup>1b</sup>, Petya K. Entcheva Campbell, Bo-Cai Gao, Larry B. Flanagan, and Michael Goulden

**Abstract**—Data from the hyperspectral imager for coastal ocean (HICO), mounted on the International Space Station (ISS), were used to develop and test algorithms for remotely retrieving ecosystem productivity. Twenty-six HICO images were used from four study sites representing different vegetation types: grasslands, shrubland, and forest. Gross ecosystem production (GEP) data from eddy covariance were matched with HICO-derived spectra. Multiple algorithms were successful relating spectral reflectance with GEP, including: spectral vegetation indices (SVI), SVI in a light-use efficiency model framework, spectral shape characteristics through spectral derivatives and absorption feature analysis, and statistical models leading to multiband hyperspectral indices from stepwise regressions and partial least squares regression. Successful algorithms were able to achieve  $r^2$  better than 0.7 for both GEP at the overpass time and daily GEP. These algorithms were successful using a diverse set of observations combining data from multiple years, multiple times during growing season, different times of day, with different view angles, and different vegetation types. The demonstrated robustness of the algorithms presented in this study over these conditions provides some confidence in mapping spatial patterns of GEP, describing variability within fields, as well as the regional patterns. The ISS orbit provides periods with multiple observations collected at different times of the day within a period of a few days. Diurnal GEP patterns were estimated comparing the half-hourly average GEP from the flux tower against HICO estimates of GEP ( $r^2 = 0.87$ ) if morning, midday, and afternoon observations were available.

**Index Terms**—Ecosystems, hyperspectral imaging, remote sensing.

## I. INTRODUCTION

**P**HOTOSYNTHESIS is possibly the most important biochemical process on Earth. It provides the energy that

powers ecosystem processes, thus it is critically important for the understanding of ecosystem function [1]. Photosynthesis is one of the key processes removing CO<sub>2</sub>, an important greenhouse gas, from the atmosphere, providing an important feedback to the climate system [2]–[5]. While it is well known that the global carbon cycle is changing [6]–[8] with terrestrial ecosystems contributing higher carbon uptake, identifying the mechanisms and locations responsible for high carbon uptake remains an important challenge for predicting future carbon–climate interactions [6], [9]. Satellite observations have the potential to provide timely data for regions where it is difficult or impossible to collect *in-situ* measurements, however the existing satellite-based observing systems cannot provide the long term, calibrated, and spectrally sensitive observations required to quantify global carbon-budget changes [10].

There is also a strong practical need to monitor photosynthetic rates in human-managed landscapes including forests, agriculture, and rangelands [11]–[15]. Increasing population with increased purchasing power intensify demands on forest and agricultural systems, while at the same time heightened environmental stresses coupled with a changing climate increase the pressures on these systems [16]–[18]. It is presently difficult to acquire timely information on productivity patterns in space and time, which leads to a critical need for new methods to monitor the ongoing changes in range, crop, and forest production. High spectral resolution remote sensing can provide temporal and spatial observations of vegetation production and the International Space Station (ISS) can be an important platform for this study as it overflies most of the world's populated and agricultural regions.

The ISS is becoming an important site for earth remote sensing by providing a platform with power, cooling, communications, and regular resupply missions for instrument transport, all factors that can simplify mission development and cost. ISS is not in a sun-synchronous orbit, making it capable of delivering observations at different times of day, providing the potential to assess both seasonal and diurnal productivity patterns. The hyperspectral imager for coastal ocean (HICO) [19] has collected high spectral resolution imagery from ISS. Spectral approaches that directly measure biochemical changes in vegetation associated with leaf pigment concentrations and photosynthetic downregulation in response to environmental stresses are utilized in this study to estimate photosynthetic CO<sub>2</sub> uptake by terrestrial vegetation. This study makes novel use of HICO data

Manuscript received July 10, 2016; revised December 7, 2016 and June 20, 2017; accepted July 4, 2017. Date of publication September 25, 2017; date of current version October 5, 2017. This work was supported by the Center for the Advancement of Science in Space through a grant for Remote Sensing from the International Space Station. (Corresponding author: Karl Fred Huemmrich.)

K. F. Huemmrich and P. K. E. Campbell are with the Joint Center for Earth Systems Technology, University of Maryland Baltimore County, Baltimore, MD 21250 USA, and also with the Goddard Space Flight Center, Greenbelt, MD 20771 USA (e-mail: karl.f.huemmrich@nasa.gov; petya.campbell@nasa.gov).

B.-C. Gao is with the Remote Sensing Division, Naval Research Laboratory, Washington, DC 20375 USA (e-mail: bo-cai.gao@nrl.navy.mil).

L. B. Flanagan is with the Department of Biological Sciences, University of Lethbridge, Lethbridge, AB T1K 3M4, Canada (e-mail: larry.flanagan@uleth.ca).

M. Goulden is with the Department of Earth System Science, University of California, Irvine, CA 92697 USA (e-mail: mgoulden@uci.edu).

Color versions of one or more of the figures in this paper are available online at <http://ieeexplore.ieee.org>.

Digital Object Identifier 10.1109/JSTARS.2017.2725825

as it is directed toward terrestrial ecosystems rather than coastal regions.

The goal of this study is the development of techniques for determining photosynthetic carbon uptake by terrestrial ecosystems, where the level of carbon uptake is determined using optical signals from sensors on ISS. To achieve this goal, we address the following science questions: Do optical signals from hyperspectral reflectance describe variations in ecosystem carbon fluxes? Are these relationships consistent over different vegetation types? Can we detect both diurnal and seasonal changes in vegetation?

## II. BACKGROUND

Ecosystem productivity can be continuously measured for a specific location using eddy covariance techniques on flux towers [20]. The flux towers measure net ecosystem exchange (NEE), the movement of carbon, in the form of CO<sub>2</sub>, between the atmosphere and the ground. NEE can be decomposed into gross ecosystem productivity (GEP), the uptake of CO<sub>2</sub> by photosynthesis and ecosystem respiration (Reco), the loss of CO<sub>2</sub> from the ecosystem into the atmosphere [21], [22]. Flux towers routinely measure net fluxes averaged over half-hourly periods, allowing examination of diurnal changes in GEP, and can be aggregated to daily and seasonal GEP values [20].

Vegetation productivity varies over multiple time scales [20], [23]. Short-term photosynthetic function responds to environmental stresses, such as low or high temperatures or water deficiency. Changes in diurnal patterns of CO<sub>2</sub> fluxes may provide early signs of impacts on plant growth. Data collected over longer periods of time reveal seasonal growth patterns in the timing and rate of springtime green up and autumn senescence. They also can show responses to transient stresses, such as to periods of drought. For agricultural systems productivity patterns over the course of a growing season provide information to derive crop yield, which is particularly sensitive to the environmental conditions during the reproductive and grain-filling periods [24], [25].

Useful information for ecologists and land managers emerges out of the ability to monitor change in range, forest, and crop production over diurnal to seasonal time periods. Descriptions of spatial variations are also important to these users. ISS can provide a sensor platform for remote sensing, collecting data at various temporal, and spatial scales that can address these needs.

Leaf pigment concentrations play an important role in plant photosynthesis and protection. Pigment concentrations can be estimated using spectral reflectance measurements [26]–[28], including observations from orbit [29], [30]. Pigment levels vary with plant physiological status and their variability can identify periods of stress and reduced photosynthetic activity. There are three major classes of plant pigments: chlorophylls, carotenoids, and anthocyanins [26], [28]. Variations in the pigment concentrations, control potential photosynthesis, describe levels of photoprotection, and provide an indirect estimate of plant nutrient status [31]–[33].

In circumstances when the leaf absorption of photosynthetically active radiation (PAR) exceeds the capacity of the

photosynthetic processes to use that energy, reactions in the xanthophyll cycle cause the pigment violaxanthin to reverse epoxidation and form zeaxanthin via antheraxanthin. This process protects the leaf's photosynthetic biochemical machinery by releasing excess energy as heat [34], [35]. The spectral properties of these pigments cause an observable change in leaf reflectance at 531 nm as the relative amounts of the different xanthophyll pigments varies [36]–[38]. The photochemical reflectance index (PRI) is designed to detect this reaction, although the PRI signal is also affected by carotenoid and chlorophyll pigment concentrations and conformational changes in the chloroplasts [39]. PRI is a normalized difference ratio of two narrow visible wavelengths (typically, 531 nm—the detection band and a reference band at 570 nm). A number of field and remote-sensing studies have demonstrated that PRI is strongly related photosynthetic light-use efficiency (LUE) at leaf and canopy levels [34], [40]–[48]. PRI calculated from orbital observations using Hyperion hyperspectral imagery [30], [49] was strongly associated with vegetation photosynthetic function for both hardwood and conifer forest sites [30].

Terrestrial vegetation responds to changing environmental conditions at diurnal and seasonal timescales. The magnitude, rate, and duration of these responses are related to ecosystem processes, such as carbon balance and evapotranspiration. Diurnal responses are the least well understood and least explored by present remote-sensing science. Stress responses over a day can result in significant decreases in daily GEP. For example, observations made only at 10 AM, the nominal overpass time for Terra and Landsat, may indicate a little plant stress, while an observation made later in the day could show much higher stress levels in response to higher temperatures, drier air, and increased light levels. These discrepancies accumulate when calculating annual GEP for yield estimations, resulting in significant uncertainties. Thus, the use of multiple observations from different times of day (as is possible from ISS HICO) may improve understanding of stress responses that foreshadow a decline in agricultural yield and serious disturbance events such as fires or insect outbreaks.

Current satellite systems do not provide the frequent high-resolution narrow band spectral observations required to study vegetation physiological dynamics. ISS-mounted sensors, such as HICO, are able to collect repeatable observations of widely distributed sites through the growing season and at different times of the day to observe vegetation over a range of different illumination and stress conditions to address these plant physiology questions.

## III. METHODS

### A. HICO Spectral Data

HICO was a pushbroom sensor mounted on ISS with a 350–1080-nm spectral range, 5.7-nm spectral sampling, and a signal-to-noise ratio (SNR) greater than 200:1 for a 5% albedo scene [19], [50]. It had a spatial resolution of approximately 100 m, depending on the altitude of the ISS and the elevation of the terrain [51]. These characteristics made HICO a good choice for this study as its spectral range, resolution, and SNR

TABLE I  
DESCRIPTION OF THE HICO IMAGERY USED IN THIS STUDY

Scene ID	Date (GMT)	Time (GMT)	Solar Zenith Angle	Solar Azimuth Angle	View Angle from Nadir	View Azimuth Angle	Site
11230	08/29/12	20:44:00	42.9	206.5	-17.6	159.5	Lethbridge
11239	08/30/12	21:32:00	47.7	221.8	25.6	353.6	Lethbridge
11260	09/01/12	23:09:00	61.2	246.7	-13.1	199.7	Lethbridge
11289	09/03/12	21:32:00	49.3	222.0	20.2	9.9	Lethbridge
11303	09/04/12	20:43:00	45.2	206.1	27.8	2.1	Lethbridge
13961	06/28/13	23:41:00	54.2	264.6	7.7	14.6	Lethbridge
13972	06/29/13	21:15:00	32.6	225.7	24.7	352.1	Lethbridge
14000	07/01/13	22:51:35	39.1	240.8	11.2	13.5	Lethbridge
14014	07/02/13	22:02:39	46.3	253.6	-7.7	198.6	Lethbridge
14677	09/12/13	15:54:00	39.1	240.8	11.2	13.5	Lethbridge
16054	04/29/14	22:57:00	55.1	248.9	5.0	15.4	Lethbridge
16462	06/20/14	23:15:00	50.2	259.7	-10.4	161.1	Lethbridge
16511	06/25/14	23:59:00	57.3	268.5	17.4	11.0	Lethbridge
16582	07/01/14	22:21:00	41.8	246.1	-10.4	199.3	Lethbridge
16682	07/10/14	15:01:00	59.4	90.7	-30.8	157.1	Lethbridge
16697	07/11/14	17:26:00	37.6	124.6	24.4	6.2	Lethbridge
17087	08/27/14	23:27:00	62.0	251.8	3.0	15.9	Lethbridge
10769	07/07/12	16:29:03	46.9	89.4	27.9	319.3	CA-Grassland/Coastal Sage
11326	09/06/12	23:57:35	62.9	258.8	35.8	223.2	CA-Grassland/Coastal Sage
13314	04/22/13	21:38:18	32.3	234.7	26.1	319.2	CA-Grassland/Coastal Sage
13323	04/23/13	20:47:40	24.5	214.1	28.5	137.1	CA-Grassland/Coastal Sage
15045	10/31/13	17:17:45	57.8	138.9	16.5	137.5	CA-Grassland/Coastal Sage
16619	07/05/14	15:49:09	55.2	83.7	25.0	318.9	CA-Grassland/Coastal Sage
2201	03/18/10	21:41:23	48.8	205.3	41.6	147.2	Marys River Fir
3489	07/25/10	17:08:59	47.1	105.3	42.4	147.0	Marys River Fir
6640	05/20/11	15:56:15	58.0	93.1	4.2	151.3	Marys River Fir

meet the requirements for optical determination of plant pigment concentrations, and its spatial resolution was similar in scale to the observation footprint of the flux towers. HICO collected imagery from September 2009 to September 2014, when the instrument failed.

The HICO imagery used in this study are listed in Table I. For the primary study site with the largest number of HICO images, the study used 17 images acquired over three years (2012–2014) for the region around the flux tower located in a grassland site near Lethbridge, AB, Canada (49.7092°N, 112.9403°W) [52], [53]. We focused on this site because of its location near the northernmost extent of the ISS orbit increased the opportunities to study diurnal change (see below). Unfortunately, the failure of HICO during this project limited the number of images we could collect for analysis. To examine other sites and vegetation types, we also made use of existing imagery that observed sites with operating flux towers. These secondary sites included: two sites that are part of the Southern California Climate Gradient study, Coastal Sage (CA-Coastal Sage, 33.734°N, 117.696°W), and Grassland (CA-Grassland, 33.737°N, 117.695°W) both in Southern California; and a Douglas fir Ameriflux site at Marys River, Oregon (44.6465°N, 123.5515°W).

### B. ISS Orbits and Data Collection

The ISS orbit affects the timing of observations, which is important for understanding its ability to sample the continuous series of CO<sub>2</sub> fluxes. Unlike most remote-sensing satellites, ISS is not in a sun-synchronous orbit. ISS moves west to east in a 51.6° inclination orbit with each orbit shifting westward by approximately 22.9° of longitude from the previous

orbit. Orbital tracks over the same ground site repeat about every three days. However, overpasses occur at different times of the day, so solar illumination angles vary for every site observation. The ISS orbit produces a pattern of daylight overpasses that follows an approximate 63-day cycle, which can be divided into approximately four two-week long periods. For the first two weeks, ISS is always in darkness when it passes over the northern hemisphere, in the next two weeks, there is an even split in daylight observations between the northern and southern hemispheres, the following two weeks, ISS is always in darkness when it passes over the southern hemisphere, and in the last two weeks, there is an even split again (see Fig. 1) (<http://eol.jsc.nasa.gov/Tools/orbitTutorial.htm>, [54]). This characteristic of the ISS orbit results in a distinct pattern for the timing of daylight overpasses of sites depending on their location. Near the poleward extremes of the orbital coverage, daytime overpasses are clumped over a few days with periods between with no daytime overpasses. During the periods of daytime overpasses, the overpass times begin with afternoon observations and become earlier in subsequent orbits (top plot, Fig. 2). Moving toward the equator, there is less clumping in the timing of the daytime overpasses (bottom plot, Fig. 2).

These temporal patterns of daylight overpasses affect the use of ISS optical data for descriptions of seasonal vegetation growth and phenology, as data gaps may occur during important periods of vegetation activity, as illustrated in Fig. 2, which shows seasonal normalized-difference vegetation index (NDVI) curves along with dates of potential observations (if conditions are clear for the overpass). Furthermore, in this study, HICO could not collect observations of the sites at every opportunity due to



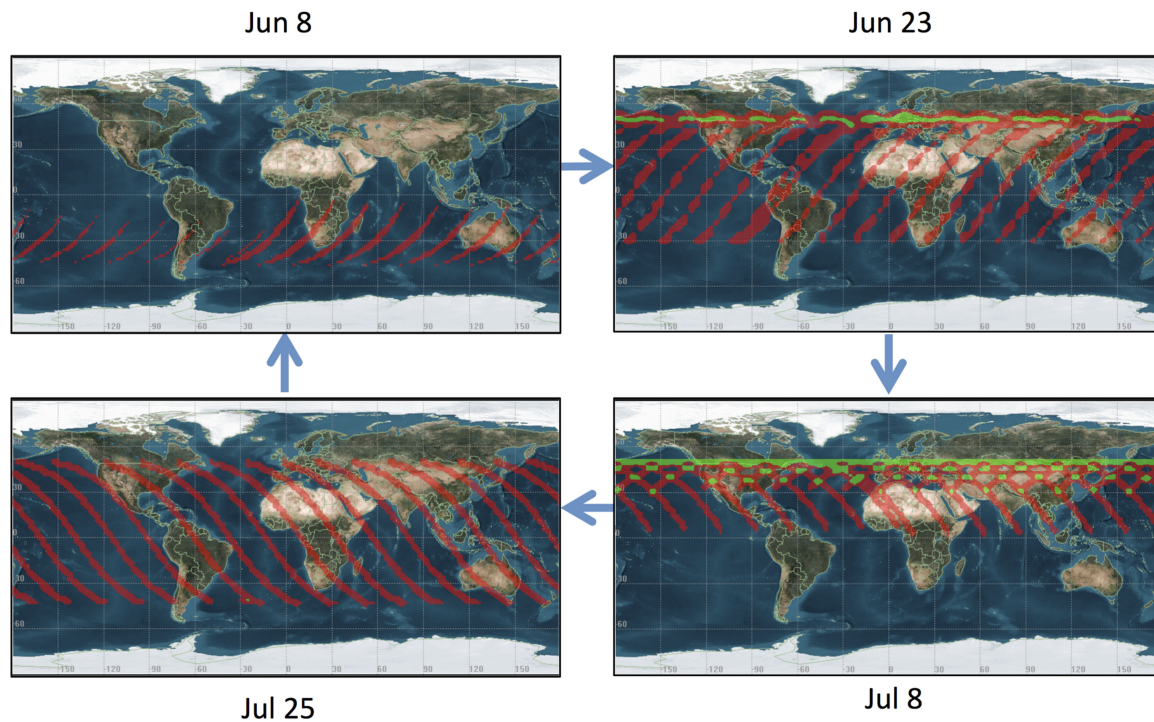


Fig. 1. Potential daylight views for ISS orbits (red points for single view and green points for two or more views) for selected days showing a cycle of daytime ground observation opportunities. The precise patterns will vary from year to year, depending on the ISS orbit altitude, but the general pattern remains consistent.

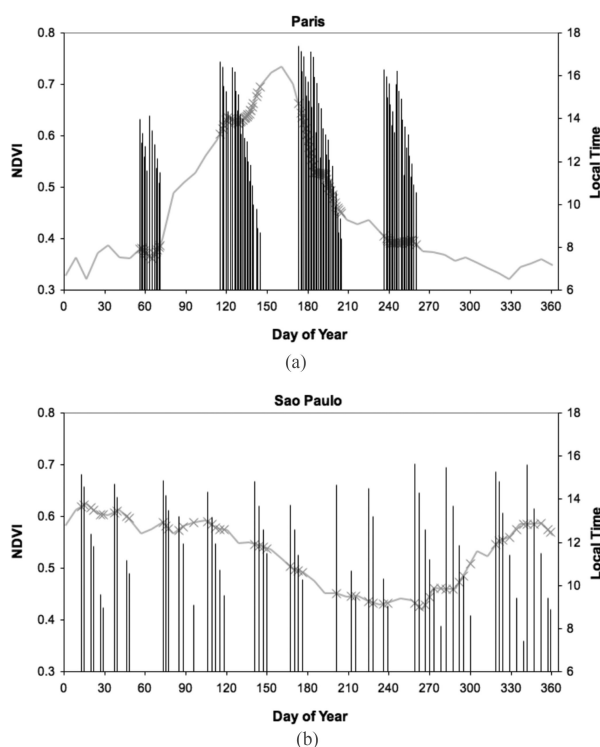


Fig. 2. ISS daytime overpasses for two sites: (a) One near the northernmost part of the orbit (top plot, Paris at 48.9°N) and (b) one nearer to the equator (bottom plot, São Paulo at 23.5°S). Vertical lines show days with daytime overpasses where the line height indicates overpass times. These are general patterns for the overpasses, the exact dates and times of overpasses will vary with changes in the ISS orbit. The black curves are a ten-year average MODIS NDVI for the areas, and the “X” symbols note the NDVI for the day of the potential ISS observations.

clouds or operational conflicts with collections at other sites, yet the timing of the available HICO images does match up with the patterns shown in Fig. 2. All of this study’s HICO imagery were collected near days 60, 120, 180, 240, and 300, and these data collection periods were separated by approximately 60-day intervals as described above (see Fig. 3). This results in important limitations on the use of ISS-mounted sensors for studying ecosystem responses. For example, there are no observations of the Lethbridge site during the period of seasonal maximum GEP, nor observations to describe the start of springtime green up, two critical variables for determining seasonal GEP (see Fig. 3). Another example is the lack of daylight observations in winter, which means no data were available during the most productive periods for the California sites (see Fig. 3).

### C. HICO Data Processing

HICO’s top of atmosphere radiances were converted to surface reflectance using the well-established ATmosphere RE-Moval (ATREM) algorithm [55], developed for pushbroom imaging spectrometers with cross-track spectral calibration variations. ATREM was designed to account for the differences in illumination geometry associated with the varying off nadir looks of HICO (see Table I), and has been extensively tested for correction of HICO data collects of various land covers. ATREM uses the 6S radiative transfer model [56], constrained by the date, time of day, elevation, and observation geometry, to account for the changes in solar illumination, and explicitly simulate the absorption and scattering effects of atmospheric gases and aerosols.

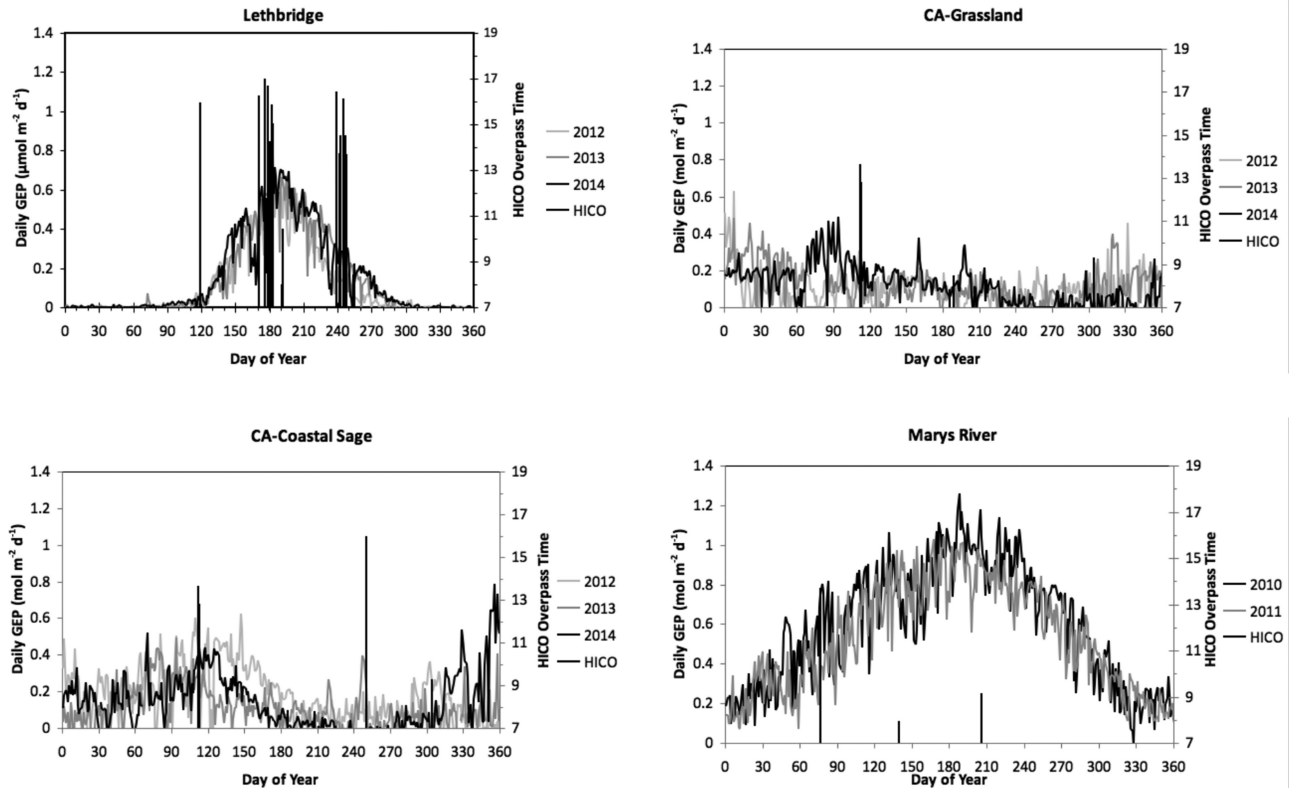


Fig. 3. Seasonal patterns of daily GEP from flux tower measurements for the four study sites. The position of the vertical black lines indicates dates of HICO imagery, and the height of the vertical lines shows the local time of day of the overpasses. The four plots are: Lethbridge data in upper left plot; CA-grassland in upper right plot; CA-coastal sage in lower left plot; and Marys River in lower right plot.

The images were visually evaluated, areas of uniform vegetation cover around the flux towers were located, and reflectance spectra from pixels free of clouds or cloud shadows were extracted. Depending on the site, view angles, and cloud conditions, between 7 and 25 pixels from an image were sampled and averaged for each spectral extraction. Sample surface reflectance spectra are shown in Fig. 4.

#### D. Flux Data and Processing

All of the study sites have operating flux towers where  $\text{CO}_2$ , water, and energy fluxes are measured using eddy covariance methods [57], [58]. The measured NEE values were partitioned into Reco and GEP. The Lethbridge data were processed using the Fluxnet-Canada standard protocols for gap filling and partitioning eddy flux  $\text{CO}_2$  data [59]. The CA site data were processed following procedures described in [60]. Marys River site data were processed using Ameriflux protocols [21], [22], [61], [62]. Half-hour average GEP values were matched by date and time with the HICO image extractions. Half-hourly GEP values at the times of the overpasses ranged from 0 to  $26.6 (\mu\text{mol}\cdot\text{m}^{-2}\cdot\text{s}^{-1})$ . Daily GEP values were also calculated (see Fig. 3) and matched with the spectral data. Daily GEP values for the observation days were between 0 and  $1.04 (\text{mol}\cdot\text{m}^{-2}\cdot\text{d}^{-1})$ .

The flux towers also routinely collect a suite of meteorological measurements including: air temperature, humidity,

soil temperature, wind speed and direction, air pressure, and incident PAR. On three of the towers (Lethbridge, CA-grassland, and CA-coastal sage), there are radiation sensors that can be used to calculate NDVI values [63], [64].

As a test of the atmospheric correction, NDVI calculated from HICO spectra

$$\text{NDVI} = (R_{805} - R_{668}) / (R_{805} + R_{668}) \quad (1)$$

where  $R_{xxx}$  refers to the reflectance of the HICO band at wavelength xxx nm, and ground measured NDVI from radiation sensors on the flux towers collected at the times of ISS overpasses were compared. The correlation for the Lethbridge data is 0.95 and for the CA sites is 0.86. These strong correlations indicate the quality of the HICO surface reflectance retrievals.

The study sites have distinctly different ecosystem characteristics as shown in their seasonal patterns of GEP (see Fig. 3). The Lethbridge site is a short grass prairie responding to a climate with cold winters and hot summers resulting in rapid green up in the spring and a fairly short growing season [53]. The two CA sites are in a warm temperate Mediterranean climate, with hot and very dry summers, thus both have green canopies and most of their productivity in the winter and spring with low summer GEP values. The Marys River site is dominated by evergreen conifers, mainly Douglas firs, which have green leaves all year long. This forested site is far more productive than the grassland sites and maintains productivity all through the year, although with lower productivity in the winter.

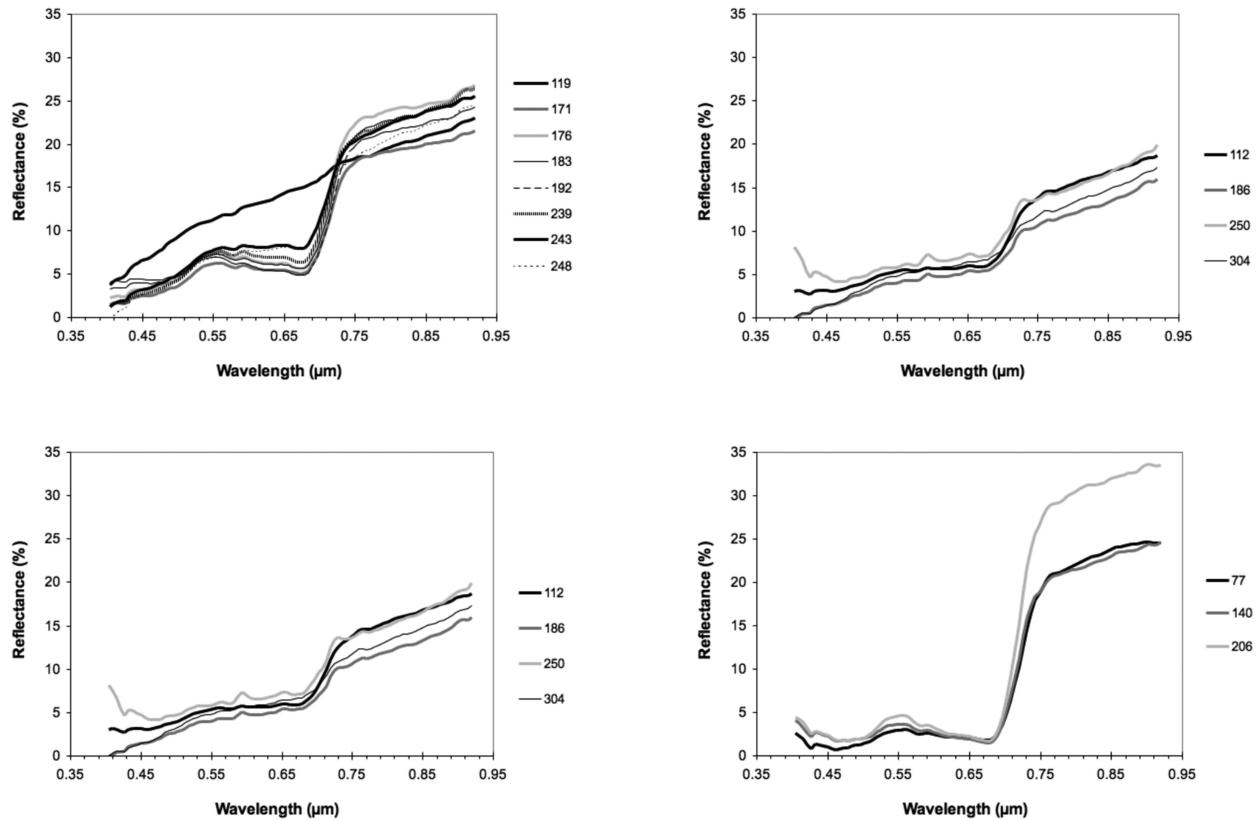


Fig. 4. Example site mean surface reflectance from HICO at the study sites for different days of the year (described in plot legends). Reflectance spectra for selected days at the Lethbridge site are shown in the upper left plot; for the CA-grassland site in the upper right plot; for the CA-coastal sage site in the lower left plot; and for Marys River site in the lower right plot.

### E. Estimation of GEP Through Remote-Sensing Models

Our objectives are using the spectral information to develop robust algorithms for estimating GEP that are applicable at multiple times of the day, different times in the growing season, and over different sites with different vegetation types. We evaluated multiple spectral approaches using individual indices, a combination of spectral factors, and the complete HICO spectral range, to obtain model formulations between HICO reflectance parameters and tower-measured GEP. These approaches include:

1) *Spectral Vegetation Indices (SVI)*: SVI are algebraic combinations of a few spectral bands, and SVI are the most popular approach for using remotely sensed data to study vegetation. Numerous studies have demonstrated relationships between SVI and plant pigments and structure (e.g., leaf area index) [65], which determine potential GEP. Vegetation LUE models can provide a useful framework for using SVI for remote sensing of GEP, because their entire set of input parameters can in principle be derived from remotely sensed measurements.

2) *Spectral Shape Descriptors*: These approaches take advantage of HICO's hyperspectral imagery by measuring the shape of the reflectance spectra. The spectral shape is affected by pigments in leaves, such as in the chlorophyll absorption feature, and is, thus, related to leaf biochemistry. Curvature of the reflectance spectra is described using derivatives and pigment absorption features are described using a continuum removal technique [30], [66].

3) *Multiband Hyperspectral Indices (MHI)*: MHI have the form

$$\text{MHI} = \sum a_i R_i \quad (2)$$

where the coefficients ( $a_i$ ) for the reflectance in specific wavelength bands ( $R_i$ ) are determined using forward stepwise multiple regression on training subsets of the data [67].

4) *Partial Least Squares Regression (PLSR)*: PLSR has successfully been used in the remote sensing of vegetation pigments and biochemistry [68]–[70]. It was developed to handle cases with few samples and many predictor variables and makes use of all the spectral bands. We developed PLSR algorithms using all spectral bands between 398 and 920 nm.

The Lethbridge site has the most observations covering the growing season, so it served as a training site for the development of MHI and PLSR, with the results tested on the three additional sites.

## IV. RESULTS

### A. Results From SVI

Multiple SVI that make use of different spectral bands were tested and several were found to be successful in describing GEP from the flux tower. In linear regressions with half-hourly GEP at time of overpass indices with  $r^2$  greater than 0.7 include (see Table II): Enhanced vegetation index (EVI) [71], the MERIS

TABLE II  
PERFORMANCE OF DIFFERENT APPROACHES RELATING INDICES DERIVED FROM HICO SPECTRAL REFLECTANCE AGAINST HALF-HOURLY AND DAILY GEP AS INDICATED BY THE COEFFICIENT OF DETERMINATION FOR LINEAR REGRESSION ( $r^2$ ) AND STANDARD ERROR OF THE REGRESSION

Name	Equation	$r^2$ Half-hourly GEP	Standard Error Half-hourly GEP ( $\mu\text{mol}\cdot\text{m}^{-2}\cdot\text{s}^{-1}$ )	$r^2$ Daily GEP	Standard Error Daily GEP ( $\text{mol}\cdot\text{m}^{-2}\cdot\text{d}^{-1}$ )
MTCI [72]	$(R753 - R708)/(R708 - R679)$	0.720	3.95	0.682	0.168
EVI [71]	$2.5 \times (R816 - R690)/(R816 + 6 \times R690 - 7.5 \times R507 + 1)$	0.745	3.76	0.828	0.123
OSAVI [73]	$1.16 \times (R805 - R673)/(R805 + R673 + 0.16)$	0.749	3.73	0.801	0.133
Chlorophyll Index [74], [75]	$(1/R713 - 1/R794) \times R794$	0.783	3.47	0.735	0.153
CCI [76]	$(R530 - \text{AVERAGE}(R622 : 668))/(R530 + \text{AVERAGE}(R622 : 668))$	0.785	3.46	0.885	0.101
APAR Eqs. (3) and (4)	$(1.45 \times \text{NDVI} - 0.218) \text{ PAR}$	0.722	3.93	0.872	0.106
f(PRI) APAR (half-hourly GEP) [30], [34], [40]–[48]	$\text{APAR} \times 0.0162 \times \text{EXP}(11.648 \times \text{PRI})$	0.744	3.77		
f(PRI) APAR (Daily GEP) [30], [34], [40]–[48]	$\text{APAR} \times 0.0189 \times \text{EXP}(12.673 \times \text{PRI})$			0.822	0.125
First Derivative at 559 nm (see Fig. 7)	$D559$	0.736	3.83	0.885	0.101
First Derivative at 736 nm (see Fig. 7)	$D736$	0.800	3.33	0.831	0.122
Dmax [79], [30]	$\text{Max}(D633:D805)$	0.677	4.24	0.771	0.142
Derivative Ratio Index [83]	$D731/D708$	0.715	3.98	0.747	0.149
Chlorophyll Absorption Feature Depth [84], [30]	PRISM [66]	0.704	4.06	0.774	0.141
Chlorophyll Absorption Feature Width at Half Maximum [84], [30]	PRISM [66]	0.528	5.12	0.525	0.205
Chlorophyll Absorption Feature Area [84], [30]	PRISM [66]	0.774	3.55	0.791	0.136

In the Equation column  $R_{xxx}$  refers to the reflectance at wavelength band xxx nm,  $D_{xxx}$  refers to the first derivative at wavelength band xxx. For all cases  $p < 0.001$ .

terrestrial chlorophyll index (MTCI) [72], and the optimized soil adjusted vegetation index (OSAVI) [73]. In addition, we examined the Gitelson chlorophyll index [74], [75], an index that uses a near-infrared band and a band on the vegetation reflectance red edge (see Table II). Since HICO hyperspectral data provide a number of spectral bands in the red edge we were able to evaluate ten bands between 701 and 753 nm, finding the 713-nm band provided the best description of both daily GEP and GEP at the overpass time (see Table II and Fig. 5).

A further advantage of using narrow-band hyperspectral imagery is the ability to simulate the responses of multiband instruments. The chlorophyll-carotenoid index (CCI) [76] was developed using MODIS spectral bands. Averaging multiple HICO bands together approximated the MODIS band responses in the CCI calculation (see Table II). CCI performed well in this study ( $r^2 = 0.78$ ) providing a cross-instrument test of this SVI.

Not only do these indices described above perform well for the half-hourly GEP, they also provide good descriptions of the daily GEP (see Table II).

Another approach for linking the SVI with GEP is through the framework of the LUE model. The basic form of the model is

$$G = \varepsilon \text{fPAR} Q_{\text{in}} = \varepsilon \text{APAR} \quad (3)$$

where  $G$  is the GEP;  $Q_{\text{in}}$  is the incoming PAR,  $\text{fPAR}$  is the fraction of PAR absorbed by vegetation;  $\text{APAR}$  is the PAR

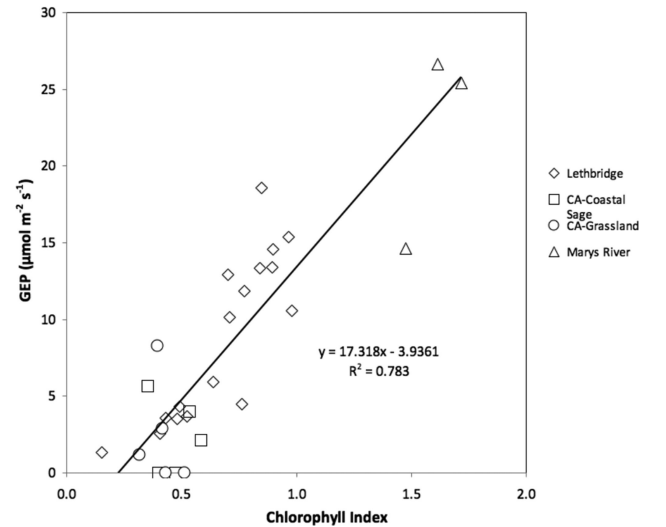


Fig. 5. Gitelson chlorophyll index  $[(1/R713 - 1/R790) \times R790]$  [74], [75] versus half-hourly GEP. Symbol shape denotes site where data were collected.

absorbed by vegetation or the product of  $\text{fPAR}$  and  $Q_{\text{in}}$ ; and  $\varepsilon$  is the LUE [77], [78].  $\text{fPAR}$  was estimated based on the seasonal patterns of NDVI and GEP for Lethbridge (upper left plot in Fig. 3) using a linear relationship with NDVI from HICO

$$\text{fPAR} = 1.455 \times \text{NDVI} - 0.218. \quad (4)$$



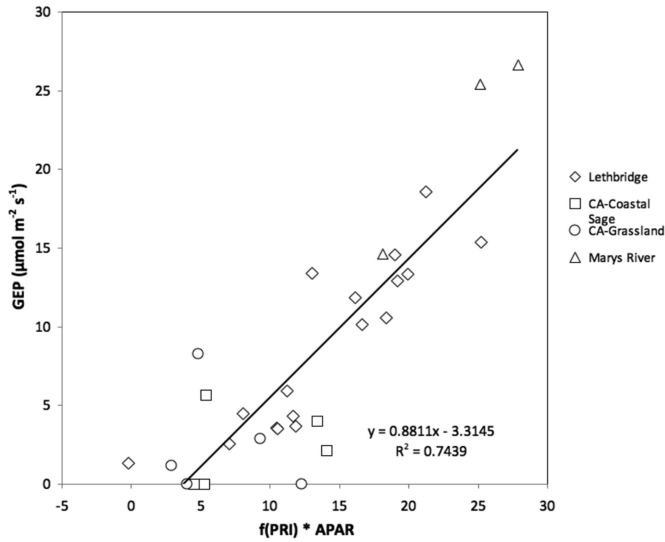


Fig. 6. Half-hourly GEP modeled by a LUE model using APAR calculated using NDVI and ground-measured incident PAR with a variable LUE calculated from PRI describes 74% of the variance in tower-measured GEP for all sites and 78% for Lethbridge alone.

This algorithm was applied to data from all sites, and combining fPAR with tower-measured half-hourly values of incident PAR to derive APAR results in a  $r^2 = 0.72$  with half-hourly GEP. Flanagan *et al.* [53] found a strong seasonal hysteresis in the APAR-GPP relationship at the Leithbridge site between the green up and senescence phases. These differences within the growing season were not detected in this study because the HICO images were collected at essentially two time periods in the growing season, not observing the full range of seasonal change.

The APAR-GEP relationship basically assumes a constant  $\varepsilon$  in (3). The GEP estimation may be improved by calculating a variable  $\varepsilon$  from PRI [43]:

$$\text{PRI} = (R_{530} - R_{570}) / (R_{530} + R_{570}). \quad (5)$$

The PRI response to  $\varepsilon$  was trained using Lethbridge data and applied to all sites. The addition of a variable  $\varepsilon$  improves the  $r^2$  with half-hourly GEP to 0.74 for all sites and up to 0.78 for Lethbridge alone (see Fig. 6). Daily values of incident PAR were used in the LUE model for daily GEP yielding a  $r^2$  of 0.82 (see Table II). The small improvement by adding in PRI reflects similar results based on ground-based measurements at the Lethbridge site by Flanagan *et al.* [53]. They suggest that much of the PRI variation in at this site is due to the effects of the varying leaf area, not leaf level biochemical changes, and so PRI provides a little new information on GEP for this site.

These results show how GEP can be estimated using a variety of different SVI. These SVI make use of a number of different spectral bands, suggesting that information in the spectral reflectance describing plant biochemistry as it affects production is distributed throughout the spectrum. Apparently, the spectral features detected by the different SVI covary providing similar results deriving GEP under the conditions observed in this dataset.

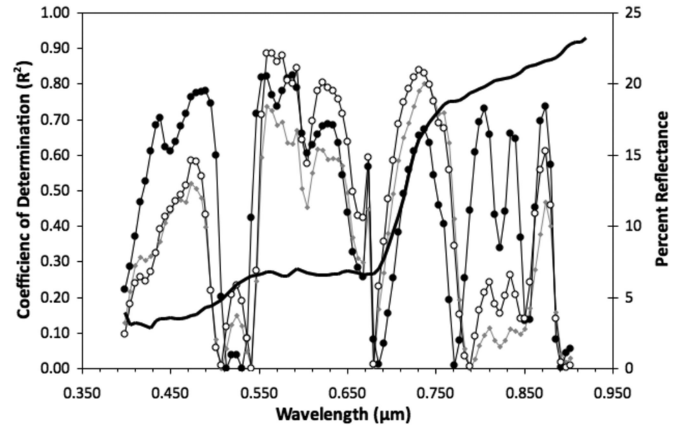


Fig. 7. Coefficient of determination ( $r^2$ ) for first derivatives of HICO spectral reflectance versus GEP. Gray points are  $r^2$  for half-hourly GEP from Lethbridge values only, solid black points are  $r^2$  for half-hourly GEP for all sites, and open circles are  $r^2$  for daily GEP for all sites. The heavy black line is the average spectral reflectance for reference.

## B. Results From Analysis of Spectral Shape

1) *Derivative Analysis:* Pigment concentrations in leaves and the overall amount of leaves affect the shape of the spectral curve, and, therefore, can provide information on the physiological processes controlling production. Derivatives of the spectral reflectance are one method to describe the spectral shape [79], [30]. Derivatives also can dampen the effect of brightness variations in the data that may be a source of noise [80], [81]. Derivatives of the HICO spectra were calculated using five-point linear Savitzky–Golay filter [82].

Fig. 7 shows the  $r^2$  of the first derivative of the HICO reflectance spectra and half-hourly GEP for the Lethbridge observations alone and for all observations. There are multiple wavelength regions with high  $r^2$  values, and the best performing band for Lethbridge was at 587 nm ( $r^2 = 0.82$ ). However, for all sites combined the  $r^2$  at 587 nm, drops to 0.63, and the best band for all sites is at 736 nm ( $r^2 = 0.80$ ) (see Fig. 7, Table II).

Dmax, the maximum value of the first derivative in the 650–750-nm range, has been proposed as a metric describing leaf chlorophyll concentration and related to GEP [79], [30]. The wavelength where Dmax occurs varies, however, Dmax did not perform as well as the derivative at specific bands in this study, returning  $r^2$  values of 0.52 for Lethbridge alone and 0.68 for all sites (see Table II).

Spectral shape descriptions in different spectral regions can be combined in a SVI using derivatives. An example is the Derivative Ratio Index (D731/D708) developed to detect a chlorophyll fluorescence signal out of the overall spectral reflectance [83] and has a  $r^2$  of 0.72 with half-hourly GEP (see Table II).

2) *Absorption Feature Analysis:* A continuum removal technique is used to quantify the characteristics of the chlorophyll absorption feature in the red part of the visible spectrum [84], [30]. In this technique, a continuum line is fitted across the absorption feature connecting the local reflectance maxima on either side. The continuum-removed reflectance is calculated by dividing the observed reflectance value by the reflectance

level of the continuum line at the same wavelength. This method normalizes reflectance spectra allowing comparisons of absorption features from a common baseline. The processing routines in IDL for spectroscopic measurements (PRISM) software package was used provide automated processing to produce continuum-removed reflectances, with spectral profile output having values between 0 and 1, enhancing the selected features [66].

Variables that describe the characteristics of the absorption feature are calculated from the continuum-removed reflectances. These include the feature depth, the greatest difference between the continuum-removed reflectance and the normalized continuum line; the feature width, the width of the absorption feature at half maximum of the feature depth; and the feature area, the area enclosed by the continuum removed reflectance curve and the normalized continuum line.

For the half-hourly GEP data from all sites, the feature width performed the poorest with a  $r^2$  of 0.53, while the feature depth had a  $r^2$  of 0.70, and the feature area performing the best with a  $r^2$  of 0.77 (see Table II).

### C. Results From MHI

Stepwise multiple regressions were used to pick spectral bands and determine coefficients for the MHI [67], [84]. This type of algorithm can produce very good results, for example, the MHI derived for half-hourly GEP trained on all of the data (MHIha) has an adjusted  $r^2$  of 0.86 ( $p < 0.01$ ), where

$$\begin{aligned} \text{MHIha} = & 3.55 + 0.119 R_{679} + 0.015 R_{776} \\ & - 0.007 R_{708} + 0.006 R_{404} - 0.128 R_{690}. \end{aligned} \quad (6)$$

Selection of the training data, however, is critical in any statistical modeling approach. It is important to have training data that describes the full variability in the data because omissions in the training dataset may result in poor performance of the algorithm when applied to new cases. This issue is illustrated in a simple demonstration of a MHI trained using only the Lethbridge data (MHIhl)

$$\text{MHIhl} = 17.67 - 0.025 R_{690} + 0.028 R_{479} \quad (7)$$

which provides a good description of the training data with an adjusted  $r^2$  of 0.79 but does poorly deriving GEP for the other sites, with an adjusted  $r^2$  for all sites combined dropping to 0.37 due to the structural and biochemical differences of the other sites compared to the training data.

Forward stepwise regressions were calculated using more than just the spectral reflectances, by including overpass time (Time), solar zenith, and azimuth angles, and view zenith and azimuth angles. Only the MHI for daily GEP (MHIda) was improved by including any of these other variables by adding the overpass time

$$\begin{aligned} \text{MHIda} = & -0.053 - 0.001 R_{771} - 0.002 R_{713} \\ & + 0.004 R_{547} + 0.0001 \text{Time} + 0.002 R_{805} - 0.003 R_{570} \end{aligned} \quad (8)$$

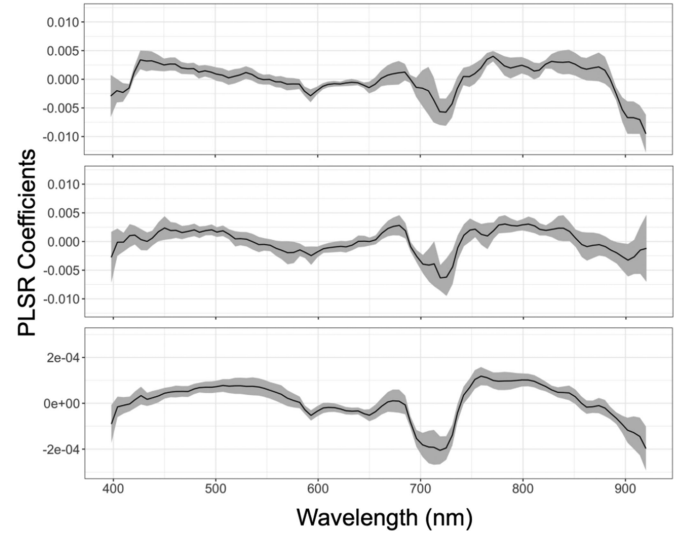


Fig. 8. Black lines are coefficients from PLSR of HICO reflectance and GEP. The lines indicate magnitude and sign of the coefficients for each wavelength band (with  $\pm 1$  standard deviation in gray). Top plot shows coefficients for half-hourly GEP at the time of the overpass for Lethbridge data alone, middle plot shows coefficients for half-hourly GEP at the time of the overpass for all sites combined, and the bottom plot shows coefficients for daily GEP for all sites combined.

resulting in an adjusted  $r^2$  for all sites of 0.94. The inclusion of Time may provide information to adjust for the different times of day as well as different solar angles when scaling from an instantaneous observation to a daily value.

### D. Results From PLSR

Rather than only using a handful of spectral bands, as the MHI do, PLSR uses information from all spectral bands. The PLSR algorithm, developed for chemical analysis spectroscopy, maximizes covariance between the independent and dependent variables, while keeping factors derived from the input spectral data orthogonal [85]. Furthermore, PLSR lends itself to cross validation more directly than the stepwise multiple regressions used to derive MHI.

A PLSR model was developed using Lethbridge data and cross validated by randomly sampling approximately two-thirds of the data (12 observations out of 17) for training, with the remaining data for testing. This process was repeated 15 times, providing an average set of coefficients with coefficient standard deviation as a description of their uncertainty (see Fig. 8, upper plot). The resulting relationship has a  $r^2$  of 0.90 and average standard error of  $1.76 \mu\text{mol} \cdot \text{m}^{-2} \cdot \text{s}^{-1}$  for half-hourly GEP of the Lethbridge training data. When the Lethbridge coefficients were applied to the other site data  $r^2$  dropped to 0.76 and the average standard error increased to  $5.13 \mu\text{mol} \cdot \text{m}^{-2} \cdot \text{s}^{-1}$ .

New PLSR coefficients were calculated for half-hourly GEP using training data sampled from all sites to evaluate possible improvement of inclusion of more diverse site information in the training. This analysis used 30 random samples of  $\sim 2/3$  of the data for training (17 of 30 observations) with the rest for testing. The derived coefficients are shown in the center plot

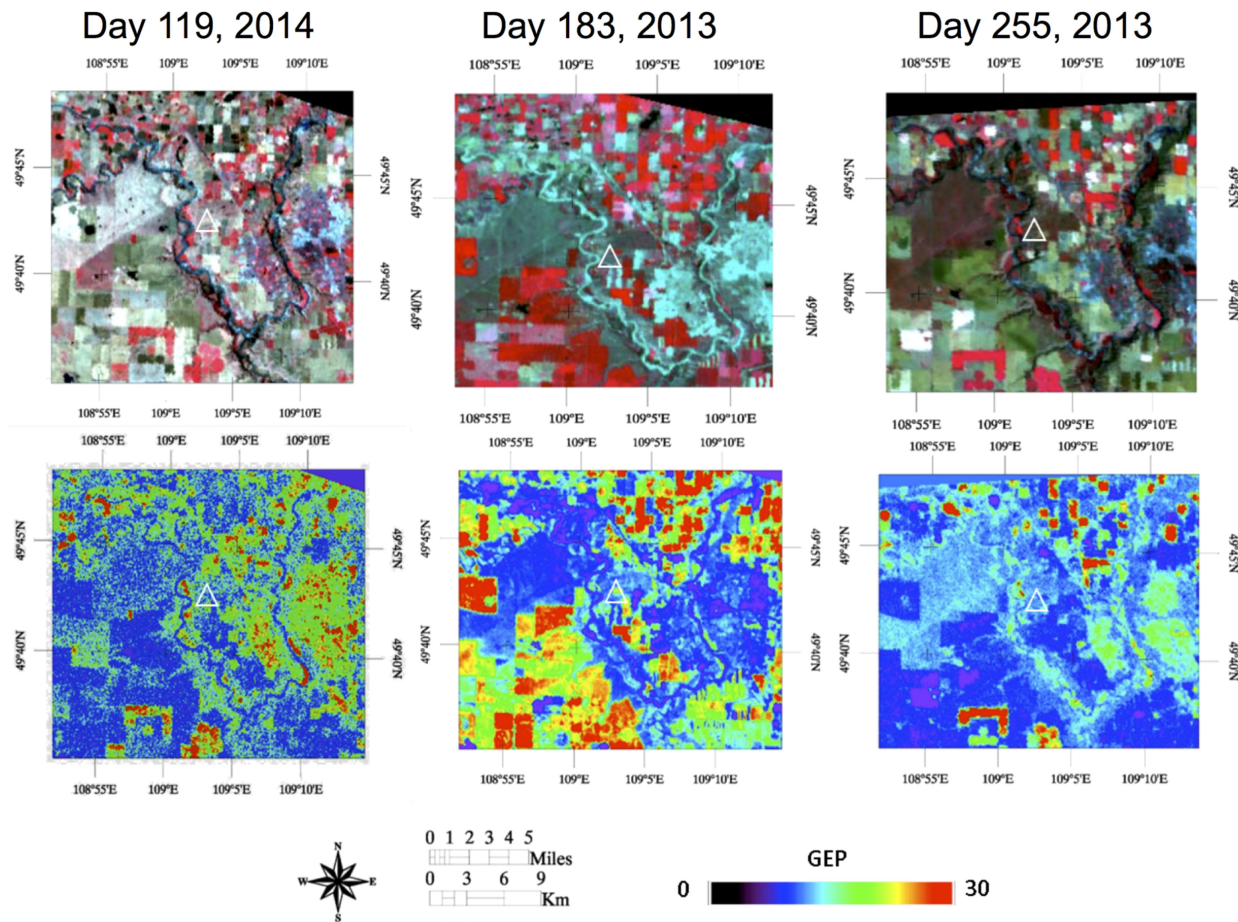


Fig. 9. Sample HICO imagery of the Lethbridge study region for three different times in the growing season showing the seasonal change and spatial heterogeneity in the region. Images in the upper row are HICO false color composites (Red:  $0.85 \mu\text{m}$ , Green:  $0.65 \mu\text{m}$ , Blue:  $0.55 \mu\text{m}$ ). Lower row has GEP images calculated from MHIha (see (6)). The location of the flux tower is noted with a white triangle in the images.

of Fig. 8. These new coefficients result in a  $r^2$  of 0.89 and standard error of  $2.63 \mu\text{mol} \cdot \text{m}^{-2} \cdot \text{s}^{-1}$  when applied to all of the data, a significant improvement over the result when using the coefficients from the Lethbridge-only training dataset, which yielded a  $r^2$  of 0.79 and standard error of  $3.63 \mu\text{mol} \cdot \text{m}^{-2} \cdot \text{s}^{-1}$ .

The same approach was also applied to calculations of daily GEP (bottom plot, Fig. 8), resulting in a  $r^2$  of 0.95 and standard error of  $0.080 \text{ mol} \cdot \text{m}^{-2} \cdot \text{d}^{-1}$ .

The PLSR coefficients derived from different training datasets produce similar curves for the different wavelength bands (see Fig. 8), particularly showing the importance of the red edge and longer wavelengths around 900-nm spectral regions in the retrieval of GEP. However, the differences in the spectral patterns of the PLSR coefficients suggest that information from different parts of the spectra may be more or less important depending on site differences or temporal scale.

### E. Mapping GEP

An important feature of the optical approaches described above is their ability, when applied to imagery, to produce maps of spatial patterns in productivity. The spatial mapping of GEP is difficult, if not impossible, using any other approach. While the algorithms are developed using data from small areas around

flux towers, these algorithms have demonstrated their robustness when they show a strong correspondence between optical signals and GEP under a variety of conditions, such as over multiple times of year, multiple years, and multiple vegetation types. Such algorithms can then be applied with some confidence on the imagery producing descriptions of both within field and regional variability in GEP.

Figs. 9 and 10 show images of GEP patterns generated using MHIha (see (6)) for areas around the study sites. The region around the Lethbridge flux tower shows the different seasonal productivity patterns for the grassland area near the tower location compared with the farmland identifiable as rectangular fields near the center of the RGB image (see Fig. 9). Furthermore, this approach is able to detect within field variability, as in the large fields southwest of the Lethbridge flux tower in the midsummer image (middle images in Fig. 9), where fields that have a uniform color in the RGB image yet show variable GEP in the lower image. The region around the Marys River site is mostly forested and the HICO-based GEP is not only sensitive to large land cover differences such as clearings but is also sensitive to variability within the intact forests (see Fig. 10). The HICO-based GEP image for the California sites shows an elevation-based gradient in productivity going up into the nearby mountains (see Fig. 10).



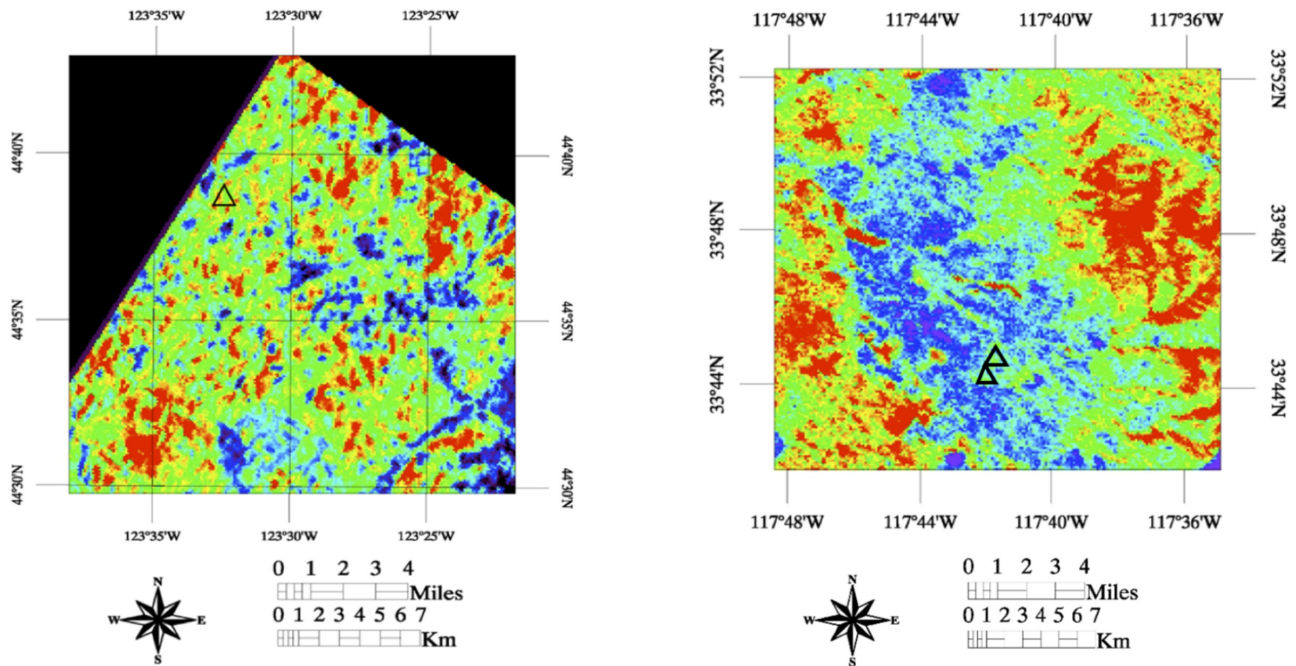


Fig. 10. Sample HICO imagery of regions around the Marys River (left image; September 4, 2012) and California grassland and coastal sage study sites (right image; July 31, 2013). Images are GEP calculated from MHIha (see (6)). The location of the flux tower is noted with black triangles in the images. The GEP color scale is the same as in Fig. 9.

#### F. Evaluating Diurnal Flux Patterns

As it is not in a sun-synchronous orbit, the ISS orbit provides an opportunity for examining diurnal GEP patterns. Over periods of a few days, where the seasonal change in GEP is small, HICO retrievals from several overpasses made at different times of the day are used to create composite diurnal patterns. Fig. 11 shows two of these periods for the Lethbridge site: days 179–183, 2013 with four observations in five days, and days 182–192, 2014 with three observations in 11 days. Both of these time periods are occurring during the latter part of canopy green up for the site (see Fig. 3). The first-order driver for diurnal GEP is varying incident PAR related to the daily movement of the sun in the sky; however, the actual GEP is also affected by the plants' ability to utilize that sunlight controlled by factors including water availability, temperature, and humidity. This is illustrated in Fig. 11 where in 2013, the midmorning GEP is higher than the midafternoon, while in 2014, the afternoon GEP is higher than the morning.

HICO-derived GEP estimates were calculated using the PLSR relationship described above. For the diurnal calculation, two other points were added, with GEP = 0 for the half hour before sunrise and after sunset. A third-order polynomial fit was used to generate a diurnal GEP pattern, shown as the smooth curves in Fig. 11. For the 2013 observations, the HICO-derived diurnal patterns do a fair job matching the ground-measured GEP, with the derived GEP well outside the standard deviation of observed GEP for much of the day and  $r^2 = 0.72$  and  $\text{RMSE} = 3.22 \mu\text{mol} \cdot \text{m}^{-2} \cdot \text{s}^{-1}$ . A weakness to this estimation of diurnal GEP is due to all of the observations being in the afternoon, and no data describing morning GEP. The 2014 case has both morning and afternoon observations (see Fig. 11) improving the HICO-derived diurnal pattern,

even though only three HICO observations were used, with  $r^2 = 0.87$  and  $\text{RMSE} = 2.07 \mu\text{mol} \cdot \text{m}^{-2} \cdot \text{s}^{-1}$ .

Vegetation responses to diurnal and short-term (minutes to hours) environmental changes may be different than seasonal growth or responses to longer term stresses. The nature and detection of these responses are important research questions, unfortunately this dataset only hints at how these issues could be explored through ISS-mounted sensors. One example is an index developed to detect anthocyanin pigment concentrations, the anthocyanin pigment index (API) [28]:

$$\text{API} = ((1/R550) - (1/R700)) \times R790 \quad (9)$$

applied to the Lethbridge data has a  $r^2$  with half-hourly GEP for all dates of only 0.16, while for the observations collected between days 171 and 192 of 2014, a brief period of the growing season with five observations with different observation times, the  $r^2$  is 0.77. This suggests algorithms that perform poorly in capturing the seasonal patterns of GEP may be sensitive to the types of vegetation responses that occur over shorter time periods. However, more sets of observations describing diurnal change are required to test these hypotheses.

#### G. Evaluating Seasonal Patterns

Descriptions of seasonal patterns of GEP are necessary to derive accurate annual carbon budgets, production, and yield estimates. However, seasonal descriptions derived from ISS-mounted instruments are problematic for this purpose. Periods without daylight overpasses result in data gaps (see Figs. 2 and 3), while variations in overpass times introduce uncertainties in calculations of midday or daily GEP (see Figs. 11 and 12). These issues are illustrated in Fig. 12, showing the seasonal



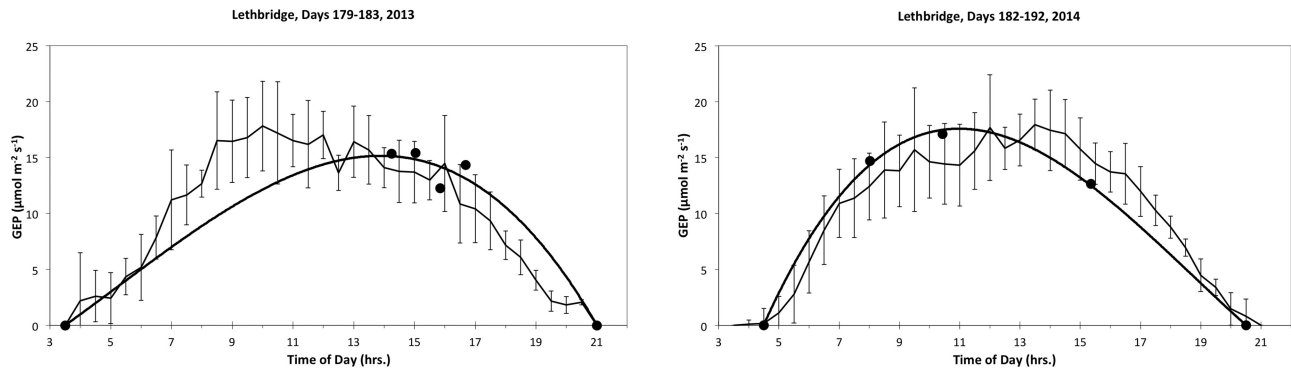


Fig. 11. Diurnal GEP patterns at Lethbridge site for two periods of the growing season with multiple HICO overpasses, with the plot for days 179–183, 2013 on the left and for days 182–192, 2014 on the right. The average diurnal GEP over the time period measured by the flux tower is the solid black line with error bars of  $\pm 1$  standard deviation. Black points are HICO estimates for GEP using the PLSR algorithm and the smooth curved line is a diurnal GEP estimate based on a polynomial fit to the HICO points.

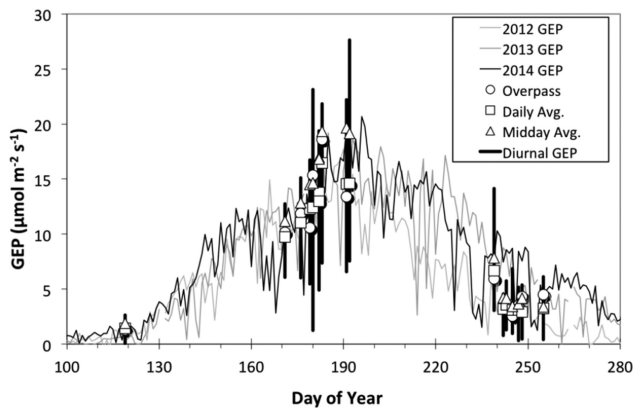


Fig. 12. Seasonal patterns of midday GEP (average of 11:30 to 13:30) from Lethbridge flux tower for the three study years (thin gray lines). HICO observation days are designated by points and vertical lines. The points indicate ground-measured GEP at the time of the ISS overpass (circles), the daily average GEP (squares), and the midday GEP (triangles). The dark vertical lines indicate the diurnal range of GEP between 7:00 and 19:00. A GEP retrieval from HICO could potentially occur at any position on those vertical lines.

patterns of midday average GEP for the Lethbridge site and the occurrence of all of the available HICO observations. For this site, near the northernmost extent of the ISS orbit, observations are clustered leaving gaps during the growing season without data for a seasonal estimate. The vertical lines in Fig. 12 show the range of half-hourly GEP values between 7:00 AM and 7:00 PM. Even with perfect retrievals of GEP from ISS observations, the timing of the overpasses can introduce a level of uncertainty in an estimate of midday or daily GEP. Addressing these issues for ISS data may require modeling based on estimates of diurnal GEP patterns, such as those described above, to estimate midday or daily flux values as well as models or data from other satellites describing seasonal patterns for filling in data gaps.

Observations in this study occur between about 8:00 AM and 5:00 PM local time and while there can be large variations in fluxes over the course of a day (see Figs. 11 and 12), in the case of this dataset, the daily GEP is highly correlated with the half-hourly GEP at the times of the overpasses ( $R = 0.93$ ). Thus, the successful algorithms for half-hourly GEP described above also perform well for daily GEP, as shown in Table II.

## V. CONCLUSION

Twenty-six HICO images were processed to retrieve surface spectral reflectance for four study sites. Each of the sites supported flux towers measuring ecosystem carbon fluxes using eddy covariance techniques and GEP data from the towers were matched with the HICO data resulting in a total of 30 observations. These data were used to successfully develop multiple approaches relating spectral reflectance with GEP, a key ecophysiological variable, including using different SVI directly, using SVI in a LUE model framework, using spectral shape characteristics through spectral derivatives and absorption feature analysis, and developing statistical models leading to MHI from forward stepwise regressions and PLSR. Furthermore, these algorithms proved to be successful using a diverse set of observations collected over multiple years, at multiple times during the growing season, at different times of the day, with different view angles, and for different vegetation types. These successes suggest that robust algorithms using spectral data can potentially produce global descriptions of ecosystem productivity.

The successful SVIs and MHI used a variety of spectral bands, and in the spectral shape analysis, the first derivative showed multiple promising spectral bands for deriving GEP. These results indicate spectral information related to productivity is not confined to single bands or small spectral regions.

Statistical model approaches, such as the MHI and PLSR, were able to produce algorithms that gave excellent results. These results hint at the promise of applying advanced data mining approaches on larger datasets for the development of new algorithms. However, in the development of statistical models, great care must be taken in the generation of training datasets. For example, in this study, a MHI, trained only on the Lethbridge data, performed poorly for the points from other sites.

Because of the demonstrated success of multiple algorithms using different approaches, future operational systems may employ an ensemble of algorithms both as a quality check to detect occurrence of outliers generated from any single algorithm and to provide a quantitative measure of uncertainty in the retrieved values.

Instruments in orbit routinely collect numerous observations providing views of globally distributed locations and repeated

observations to describe temporal change. The demonstrated robustness of the algorithms presented in this study over a range of conditions provides some confidence in their application to imagery to describe spatial patterns of ecosystem and agricultural productivity away from the flux towers. These optically based methods are a natural complement to the eddy covariance methods of measuring fluxes. Eddy covariance provides continuous measurements of a single area around the flux tower, and the optical methods applied to imagery can extend those measurements to describe spatial patterns of fluxes. Sharp transitions in production at field edges, spatial variability within larger plots, productivity within areas smaller than flux tower footprints, and productivity patterns in areas on slopes are all described in the HICO imagery (see Figs. 10 and 11), but could not be measured using eddy covariance techniques. These optically based methods may be the only way to describe within field variability in production, important information for farmers, as well as the regional patterns for land managers, and global productivity patterns for ecosystem scientists.

ISS is unusual as a satellite remote-sensing platform in its ability to observe sites at different times of day. At the Lethbridge study site, which is near the northernmost part of the ISS orbit, observation opportunities came as sets of overpasses collected in groups over a few days with different overpass times that enabled examination of diurnal variability in GEP. This study showed the potential for describing diurnal GEP patterns when both morning and afternoon observations are available. Generating accurate descriptions of diurnal change in GEP are a weak area in many ecosystem carbon exchange models. ISS observations potentially could image many sites providing data to improve model descriptions of diurnal processes. Differences between morning and afternoon GEP may provide an indication of vegetation stress responses [90]. Further research and data acquisitions are required to test this hypothesis.

The instrument viewing direction relative to the solar position affects the observed bidirectional reflectance, and, thus, the values of SVI. The bidirectional reflectance distribution function is not only affected by vegetation structure, but also by leaf biochemistry, and, thus, optical properties vary depending on leaf illumination patterns [45], [86]–[89]. Accounting for view angles can improve relationships either by using only specific viewing directions [90], or by combining information from multiple view angles [45]. In this dataset, only ten of the 30 observations could be considered near nadir, that is, have view zenith angle less than  $15^\circ$ , and view zenith angles were as large as  $42^\circ$ . Relative to the solar position, view azimuth angles were in all quadrants with a collection of both forward- and back-scattering views. Given the wide distribution of view angles in this study, there were not enough observations to stratify for viewing geometry, so all views were combined. This represents an unaccounted factor in the uncertainty of the results in this analysis. Further studies accounting for, or making use of, view angle effects will further improve the retrieval of GEP.

It is necessary to collect repeated observations throughout the year for annual estimates of GEP as well as being able to capture key periods of the growing season, such as reproductive and grain-filling periods, that are critical for determining crop yield.

However, the nature of the ISS orbit introduces limitations for developing accurate descriptions of seasonal GEP patterns. At high latitudes, such as the Lethbridge site, there are significant periods of the growing season with no daytime ISS overpasses, resulting in gaps in the time series. In the Lethbridge case, these data gaps may have been large enough to obscure the strong seasonal hysteresis in the APAR-GEP relationship observed in ground-based measurements at that site [53].

While the variability of overpass times may provide some information on diurnal changes that variability introduces uncertainties in producing a consistent series of daily or midday GEP values over a growing season (see Fig. 12). However, this study found that the algorithms were successful with daily GEP even when combining observations collected at different times of the day. For the Lethbridge site, HICO observations were able to approximate seasonal growth patterns in spite of the data gaps.

The results of this study are promising, but clearly further work is needed to further refine and validate these algorithms and test new hypotheses. Unfortunately, HICO failed in September 2014, so no longer collects imagery. The only other civilian imaging spectrometer in orbit was Hyperion on the earth observing 1 (EO-1) satellite, and EO-1 was decommissioned in the fall of 2016. ISS offers the most promising near-term pathway for advancing these applications, as it is a platform that can support advanced instrumentation, such as imaging spectrometers, and also over flies much of the earth's surface, so is capable of providing the required high-quality data covering a variety of vegetation types under a range of environmental conditions. The work in this pathfinder study can be expanded greatly using a new imaging spectrometer on ISS with a mission plan to repeatedly image a collection of the hundreds of the globally distributed flux towers presently operating. This expanded mission would be able to develop and test an operational algorithm for mapping global ecosystem productivity and quantify measurement uncertainties, such as the effects of the observation time of day or effects of view and solar angles.

An instrument on ISS alone can be used to collect data for algorithm development, but it may not be sufficient for an operational system. To achieve desired temporal and spatial coverage requires a constellation of satellites. However, ISS could be an element of such a constellation, particularly one with satellites in sun-synchronous orbits, as ISS can furnish data describing responses at different times of day and be a platform for a calibration instrument for the constellation. The narrow continuous bands of an imaging spectrometer can also be convolved to simulate responses of the wider bands of multispectral sensors. Furthermore, the narrow bands are used in many of the algorithms demonstrated in this study utilize small spectral changes (e.g., spectral shape changes) for their retrievals. Thus, there is a clear need for well-calibrated imaging spectrometers and cross-calibrated instruments in a constellation. ISS would make an excellent platform for the instrument used to calibrate the other instruments in a constellation. The ISS orbit crosses the orbits of other satellites, providing opportunities for near simultaneous observations with the other members of the constellation.

ISS is poised to become an important platform for terrestrial ecosystem studies. This study's use of imaging spectrometer data provides a first step toward an improved understanding of terrestrial ecosystem processes that may be further advanced though the use of data from future ISS-mounted instruments.

#### ACKNOWLEDGMENT

The authors would like to thank the HICO Mission Office, D. MacKenzie for the ISS orbital calculations using STK, and D. Landis for graphics help. They would also like to thank B. Law's research team for providing the Marys River AmeriFlux site data, which was supported by the U.S. Department of Energy, Office of Science, under BER Contract DE-FG02-06ER64318.

#### REFERENCES

- [1] O. Morton, *Eating the Sun: How Plants Power the Planet*. London, U.K.: Harper Collins, 2009.
- [2] P. Friedlingstein *et al.*, "Climate-carbon cycle feedback analysis: Results from the C4MIP model intercomparison," *J. Climate*, vol. 19, pp. 3337–3353, 2006, doi: [10.1175/JCLI3800.1](https://doi.org/10.1175/JCLI3800.1).
- [3] G. B. Bonan, "Forests and climate change: Forcings, feedbacks, and the climate benefits of forests," *Science*, vol. 320, pp. 1444–1449, 2008.
- [4] L. Alexander *et al.*, "Climate change 2013: The physical science basis, fifth assessment report (AR5), intergovernmental panel on climate change (IPCC) working group I (WGI)," 12th Session Working Group I, Stockholm, Sweden, Sep. 23–26, 2013.
- [5] L. Bounoua *et al.*, "Quantifying the negative feedback of vegetation to greenhouse warming: A modeling approach," *Geophys. Res. Lett.*, vol. 37, pp. L23701–L23705, 2010, doi: [10.1029/2010GL045338](https://doi.org/10.1029/2010GL045338).
- [6] A. P. Ballantyne, C. B. Alden, J. B. Miller, P. P. Tans, and J. W. C. White, "Increase in observed net carbon dioxide uptake by land and oceans during the past 50 years," *Nature*, vol. 488, no. 7409, pp. 70–72, 2012.
- [7] H. D. Graven *et al.*, "Enhanced seasonal exchange of CO<sub>2</sub> by northern ecosystems since 1960," *Science*, vol. 341, no. 6150, pp. 1085–1089, 2013.
- [8] M. Forkel *et al.*, "Enhanced seasonal CO<sub>2</sub> exchange caused by amplified plant productivity in northern ecosystems," *Science*, vol. 351, pp. 696–699, 2016.
- [9] A. A. Bloom, J.-F. Exbrayat, I. R. van der Velde, L. Feng, and M. Williams, "The decadal state of the terrestrial carbon cycle: Global retrievals of terrestrial carbon allocation, pools, and residence times," *Proc. Nat. Acad. Sci.*, vol. 113, pp. 1285–1290, 2016.
- [10] I. Levin, "Earth science: The balance of the carbon budget," *Nature*, vol. 488, no. 7409, pp. 35–36, 2012.
- [11] D. Dufranne, C. Moureaux, F. Vancutsem, B. Bodson, and M. Aubinet, "Comparison of carbon fluxes, growth and productivity of a winter wheat crop in three contrasting growing seasons," *Agriculture, Ecosyst. Environ.*, vol. 141, pp. 133–142, 2011.
- [12] H. Yao, L. Tang, R. L. Brown, D. Bhatnagar, and T. E. Cleveland, "Using hyperspectral data in precision farming applications," in *Hyperspectral Remote Sensing of Vegetation*, P. S. Thenkabail, J. G. Lyon, and A. Huete, Eds. Boca Raton, FL, USA: CRC Press, 2011.
- [13] J. Chang, M. C. Hansen, K. Pittman, M. Carroll, and C. DiMiceli, "Corn and soybean mapping in the United States using MODIS time-series data sets," *Agronomy J.*, vol. 99, pp. 1654–1664, 2007.
- [14] V. Thomas, "Hyperspectral remote sensing for forest management," in *Hyperspectral Remote Sensing of Vegetation*, P. S. Thenkabail, J. G. Lyon, and A. Huete, Eds. Boca Raton, FL, USA: CRC Press, 2011.
- [15] S. J. Goetz and S. D. Prince, "Remote sensing of net primary production in boreal forest stands," *Agricultural Forest Meteorol.*, vol. 78, pp. 149–179, 1996.
- [16] W. F. Laurance, J. Sayer, and K. G. Cassman, "Agricultural expansion and its impacts on tropical nature," *Trends Ecol. Evol.*, vol. 29, no. 2, pp. 107–116, 2014.
- [17] T. Kastner, M. J. Ibarrola Rivas, W. Koch, and S. Nonhebel, "Global changes in diets and the consequences for land requirements for food," *Proc. Nat. Acad. Sci.*, vol. 109, no. 18, pp. 6868–6872, 2012.
- [18] J. Fargione, J. Hill, D. Tilman, S. Polasky, and P. Hawthorne, "Land clearing and the biofuel carbon debt," *Science*, vol. 319, no. 5867, pp. 1235–1238, 2008.
- [19] R. L. Lucke *et al.*, "Hyperspectral imager for the coastal ocean: Instrument description and first images," *Appl. Opt.*, vol. 50, no. 11, pp. 1501–1516, 2011.
- [20] D. Baldocchi, "TURNER REVIEW No. 15. 'Breathing' of the terrestrial biosphere: Lessons learned from a global network of carbon dioxide flux measurement systems," *Aust. J. Botany*, vol. 56, no. 1, pp. 1–26, 2008.
- [21] A. R. Desai *et al.*, "Cross-site evaluation of eddy covariance GPP and RE decomposition techniques," *Agricultural Forest Meteorol.*, vol. 148, no. 6, pp. 821–838, 2008.
- [22] M. Reichstein *et al.*, "On the separation of net ecosystem exchange into assimilation and ecosystem respiration: Review and improved algorithm," *Global Change Biol.*, vol. 11, no. 9, pp. 1424–1439, 2005.
- [23] D. Baldocchi *et al.*, "FLUXNET: A new tool to study the temporal and spatial variability of ecosystem-scale carbon dioxide, water vapor, and energy flux densities," *Bull. Amer. Meteorolog. Soc.*, vol. 82, no. 11, pp. 2415–2434, 2001.
- [24] R. Hay, "Harvest index: A review of its use in plant breeding and crop physiology," *Ann. Appl. Biol.*, vol. 126, pp. 197–216, 1995.
- [25] D. B. Lobell, J. A. Hicke, G. P. Asner, C. B. Field, C. J. Tucker, and S. O. Los, "Satellite estimates of productivity and light use efficiency in United States agriculture, 1982–98," *Global Change Biol.*, vol. 8, no. 8, pp. 722–735, 2002.
- [26] G. A. Blackburn, "Hyperspectral remote sensing of plant pigments," *J. Exp. Botany*, vol. 58, no. 4, pp. 855–867, 2007.
- [27] S. L. Ustin *et al.*, "Retrieval of foliar information about plant pigment systems from high resolution spectroscopy," *Remote Sens. Environ.*, vol. 113, pp. S67–S77, 2009.
- [28] A. Gitelson, "Nondestructive estimation of foliar pigment (chlorophylls, carotenoids, and anthocyanins) contents: Evaluating a semi-analytical three band model," in *Hyperspectral Remote Sensing of Vegetation*, P. S. Thenkabail, J. G. Lyon, and A. Huete, Eds. Boca Raton, FL, USA: CRC Press, 2011.
- [29] K. Gökçaya, V. Thomas, T. Noland, H. McCaughey, and P. Treitz, "Testing the robustness of predictive models for chlorophyll generated from spaceborne imaging spectroscopy data for a mixedwood boreal forest canopy," *Int. J. Remote Sens.*, vol. 35, no. 1, pp. 218–233, 2014.
- [30] P. K. E. Campbell *et al.*, "EO-1 hyperion reflectance time series at calibration and validation sites: Stability and sensitivity to seasonal dynamics," *IEEE J. Sel. Topics Appl. Earth Obs. Remote Sens.*, vol. 6, no. 2, pp. 276–290, Apr. 2013.
- [31] I. Filella, L. Serrano, J. Serra, and J. Penuelas, "Evaluating wheat nitrogen status with canopy reflectance indices and discriminant analysis," *Crop Sci.*, vol. 35, no. 5, pp. 1400–1405, 1995.
- [32] J. A. Moran, A. K. Mitchell, G. Goodmanson, and K. A. Stockburger, "Differentiation among effects of nitrogen fertilization treatments on conifer seedlings by foliar reflectance: A comparison of methods," *Tree Physiol.*, vol. 20, no. 16, pp. 1113–1120, 2000.
- [33] G. E. Bartley and P. A. Scolnik, "Plant carotenoids: Pigments for photo-protection, visual attraction, and human health," *Plant Cell*, vol. 7, no. 7, pp. 1027–1038, 1995.
- [34] J. Grace, C. Nichol, M. Disney, P. Lewis, T. Quaife, and P. Bowyer, "Can we measure terrestrial photosynthesis from space directly, using spectral reflectance and fluorescence?" *Global Change Biol.*, vol. 13, no. 7, pp. 1484–1497, 2007.
- [35] N. C. Coops, T. Hilker, F. G. Hall, C. J. Nichol, and G. G. Drolet, "Estimation of light-use efficiency of terrestrial ecosystems from space: A status report," *BioScience*, vol. 60, no. 10, pp. 788–797, 2010.
- [36] J. A. Gamon, J. Peñuelas, and C. B. Field, "A narrow-waveband spectral index that tracks diurnal changes in photosynthetic efficiency," *Remote Sens. Environ.*, vol. 41, no. 1, pp. 35–44, 1992.
- [37] J. Peñuelas, I. Filella, and J. A. Gamon, "Assessment of photosynthetic radiation-use efficiency with spectral reflectance," *New Phytol.*, vol. 131, pp. 291–296, 1995.
- [38] E. M. Middleton, K. F. Huemmrich, Y.-B. Cheng, and H. A. Margolis, "Spectral bio-Indicators of photosynthetic efficiency and vegetation stress," in *Hyperspectral Remote Sensing of Vegetation*, P. S. Thenkabail, J. G. Lyon, and A. Huete, Eds. Boca Raton, FL, USA: CRC Press, 2011.
- [39] I. Filella, A. Porcar-Castell, S. Munné-Bosch, J. Bäck, M. F. Garbalsky, and J. Peñuelas, "PRI assessment of long-term changes in carotenoids/chlorophyll ratio and short-term changes in de-epoxidation state of the xanthophyll cycle," *Int. J. Remote Sens.*, vol. 30, no. 17, pp. 4443–4455, 2009.



- [40] J. A. Gamon, H.-L. Qiu, and A. Sanchez-Azofeifa, "Ecological applications of remote sensing at multiple scales," in *Handbook of Functional Plant Ecology*, F. Valladares and F. I. Pugnaire, Eds. New York, NY, USA: Marcel Dekker, 1999.
- [41] C. J. Nichol *et al.*, "Remote sensing of photosynthetic-light-use efficiency of boreal forest," *Agricultural Forest Meteorol.*, vol. 101, no. 2, pp. 131–142, 2000.
- [42] A. F. Rahman, V. D. Cordova, J. A. Gamon, H. P. Schmid, and D. A. Sims, "Potential of MODIS ocean bands for estimating CO<sub>2</sub> flux from terrestrial vegetation: A novel approach," *Geophys. Res. Lett.*, vol. 31, no. 10, pp. L10503–L10508, 2004.
- [43] A. F. Rahman, J. A. Gamon, D. A. Fuentes, D. A. Roberts, and D. Prentiss, "Modeling spatially distributed ecosystem flux of boreal forest using hyperspectral indices from AVIRIS imagery," *J. Geophys. Res., Atmos.*, vol. 106, no. D24, pp. 33579–33591, 2001.
- [44] S. Raddi, F. Magnani, and I. Pippi, "Estimation of light use efficiency for the prediction of forest productivity from remote sensing," in *Proc. Spectra Workshop*, 2002, vol. 474, p. 21.
- [45] T. Hilker *et al.*, "A modeling approach for upscaling gross ecosystem production to the landscape scale using remote sensing data," *J. Geophys. Res., Biogeosci.*, vol. 113, no. G3, pp. G03006–G03021, 2008.
- [46] M. F. Garbulsky, J. Peñuelas, J. Gamon, Y. Inoue, and I. Filella, "The photochemical reflectance index (PRI) and the remote sensing of leaf, canopy and ecosystem radiation use efficiencies: A review and meta-analysis," *Remote Sens. Environ.*, vol. 115, no. 2, pp. 281–297, 2011.
- [47] M. F. Garbulsky, J. Peñuelas, D. Papale, and I. Filella, "Remote estimation of carbon dioxide uptake by a Mediterranean forest," *Global Change Biol.*, vol. 14, no. 12, pp. 2860–2867, 2008.
- [48] J. Peñuelas, M. F. Garbulsky, and I. Filella, "Photochemical reflectance index (PRI) and remote sensing of plant CO<sub>2</sub> uptake," *New Phytol.*, vol. 191, pp. 596–599, 2011.
- [49] G. P. Asner, K. M. Carlson, and R. E. Martin, "Substrate age and precipitation effects on Hawaiian forest canopies from spaceborne imaging spectroscopy," *Remote Sens. Environ.*, vol. 98, no. 4, pp. 457–467, 2005.
- [50] M. D. Lewis *et al.*, "The hyperspectral imager for the coastal ocean (HICO): Sensor and data processing overview," Oceanography Div, Naval Res. Lab, Stennis Space Center, MS, USA, Rep. No. NRL/PP/7330-09-9374, 2010.
- [51] B.-C. Gao and R.-R. Li, "Spectral calibrations of HICO data using atmospheric bands and radiance adjustment based on HICO and MODIS data comparisons," in *Proc. 2010 IEEE Int. Geosci. Remote Sens. Symp.*, 2010, pp. 4260–4263.
- [52] L. B. Flanagan, L. A. Wever, and P. J. Carlson, "Seasonal and interannual variation in carbon dioxide exchange and carbon balance in a northern temperate grassland," *Global Change Biol.*, vol. 8, no. 7, pp. 599–615, 2002.
- [53] L. B. Flanagan, E. J. Sharp, and J. A. Gamon, "Application of the photosynthetic light-use efficiency model in a northern Great Plains grassland," *Remote Sens. Environ.*, vol. 168, pp. 239–251, 2015.
- [54] W. L. Stefanov, C. A. Evans, S. K. Runco, M. J. Wilkinson, and K. Willis, "Astronaut photography: Handheld camera imagery from low earth orbit," in *Handbook of Satellite Applications*, J. N. Pelton, S. Madry, and S. Camacho-Lara, Eds. New York, NY, USA: Springer, 2013, pp. 683–728.
- [55] B.-C. Gao and C. O. Davis, "Development of a line-by-line-based atmosphere removal algorithm for airborne and spaceborne imaging spectrometers," *SPIE*, vol. 3118, pp. 132–141, 1997.
- [56] S. Y. Kotchenova, E. F. Vermote, R. Matarrese, and F. J. Klemm, Jr., "Validation of a vector version of the 6S radiative transfer code for atmospheric correction of satellite data. Part I: Path radiance," *Appl. Opt.*, vol. 45, no. 26, pp. 6762–6774, 2006.
- [57] L. B. Flanagan and A. C. Adkinson, "Interacting controls on productivity in a northern Great Plains grassland and implications for response to ENSO events," *Global Change Biol.*, vol. 17, no. 11, pp. 3293–3311, 2011.
- [58] M. L. Goulden, R. G. Anderson, R. C. Bales, A. E. Kelly, M. Meadows, and G. C. Winston, "Evapotranspiration along an elevation gradient in California's Sierra Nevada," *J. Geophys. Res., Biogeosci.*, vol. 117, no. G3, pp. G03028–G03041, 2012.
- [59] A. G. Barr, T. A. Black, E. H. Hogg, N. Kljun, K. Morgenstern, and Z. Nesic, "Inter-annual variability in the leaf area index of a Boreal Aspen-Hazelnut forest in relation to net ecosystem production," *Agricultural Forest Meteorol.*, vol. 126, no. 3, pp. 237–255, 2004.
- [60] M. L. Goulden *et al.*, "An eddy covariance mesonet to measure the effect of forest age on land-atmosphere exchange," *Global Change Biol.*, vol. 12, no. 11, pp. 2146–2162, 2006.
- [61] P. C. Stoy *et al.*, "An evaluation of models for partitioning eddy covariance-measured net ecosystem exchange into photosynthesis and respiration," *Agricultural Forest Meteorol.*, vol. 141, no. 1, pp. 2–18, 2006.
- [62] B. D. Amiro *et al.*, "Carbon, energy and water fluxes at mature and disturbed forest sites, Saskatchewan, Canada," *Agricultural Forest Meteorol.*, vol. 136, no. 3, pp. 237–251, 2006.
- [63] J. A. Gamon *et al.*, "SpecNet revisited: Bridging flux and remote sensing communities," *Can. J. Remote Sens.*, vol. 36, no. Sup2, pp. S376–S390, 2010.
- [64] K. F. Huemmrich, T. A. Black, P. G. Jarvis, J. H. McCaughey, and F. G. Hall, "High temporal resolution NDVI phenology from micrometeorological radiation sensors," *J. Geophys. Res., Atmos.*, vol. 104, no. D22, pp. 27935–27944, 1999.
- [65] D. A. Roberts, K. L. Roth, and R. L. Perroy, "Hyperspectral vegetation indices," in *Hyperspectral Remote Sensing of Vegetation*, P. S. Thenkabail, J. G. Lyon, and A. Huete, Eds. Boca Raton, FL, USA: CRC Press, 2011.
- [66] R. F. Kokaly, "PRISM: Processing routines in IDL for spectroscopic measurements (installation manual and user's guide, version 1.0)," U.S. Geological Survey Open-File Report 2011b1155, 2011. [Online]. Available: <http://pubs.usgs.gov/of/2011/1155/>
- [67] P. S. Thenkabail, J. G. Lyon, and A. Huete, "Advances in hyperspectral remote sensing of vegetation and agricultural croplands," in *Hyperspectral Remote Sensing of Vegetation*, P. S. Thenkabail, J. G. Lyon, and A. Huete, Eds. Boca Raton, FL, USA: CRC Press, 2011.
- [68] G. P. Asner, R. E. Martin, C. B. Anderson, and D. E. Knapp, "Quantifying forest canopy traits: Imaging spectroscopy versus field survey," *Remote Sens. Environ.*, vol. 158, pp. 15–27, 2015.
- [69] S. P. Serbin *et al.*, "Remotely estimating photosynthetic capacity, and its response to temperature, in vegetation canopies using imaging spectroscopy," *Remote Sens. Environ.*, vol. 167, pp. 78–87, 2015.
- [70] M. E. Martin, L. C. Plourde, S. V. Ollinger, M.-L. Smith, and B. E. McNeil, "A generalizable method for remote sensing of canopy nitrogen across a wide range of forest ecosystems," *Remote Sens. Environ.*, vol. 112, no. 9, pp. 3511–3519, 2008.
- [71] A. Huete, C. Justice, and H. Liu, "Development of vegetation and soil indices for MODIS-EOS," *Remote Sens. Environ.*, vol. 49, no. 3, pp. 224–234, 1994.
- [72] J. Dash and P. J. Curran, "The MERIS terrestrial chlorophyll index," *Int. J. Remote Sens.*, vol. 25, no. 23, pp. 5403–5413, 2004.
- [73] G. Rondeaux, M. Steven, and F. Baret, "Optimization of soil-adjusted vegetation indices," *Remote Sens. Environ.*, vol. 55, no. 2, pp. 95–107, 1996.
- [74] Y. Peng and A. A. Gitelson, "Application of chlorophyll-related vegetation indices for remote estimation of maize productivity," *Agricultural Forest Meteorol.*, vol. 151, no. 9, pp. 1267–1276, 2011.
- [75] Y. Peng, A. A. Gitelson, G. Keydan, D. C. Rundquist, and W. Moses, "Remote estimation of gross primary production in maize and support for a new paradigm based on total crop chlorophyll content," *Remote Sens. Environ.*, vol. 115, no. 4, pp. 978–989, 2011.
- [76] J. A. Gamon *et al.*, "A remotely sensed pigment index reveals photosynthetic phenology in evergreen conifers," *Proc. Nat. Acad. Sci.*, vol. 113, no. 46, pp. 13087–13092, 2016.
- [77] J. L. Monteith, "Climate and efficiency of crop production in Britain," *Philosoph. Trans. Roy. Soc. London B, Biol. Sci.*, vol. 281, no. 980, pp. 277–294, 1977.
- [78] G. Russell, P. G. Jarvis, and J. L. Monteith, "Absorption of radiation by canopies and stand growth," in *Plant Canopies: Their Growth, Form and Function*, G. Russell, B. Marshall, and P. G. Jarvis, Eds. Cambridge, U.K.: Cambridge Univ. Press, 1989.
- [79] G. A. Blackburn, "Quantifying chlorophylls and carotenoids at leaf and canopy scales: An evaluation of some hyperspectral approaches," *Remote Sens. Environ.*, vol. 66, no. 3, pp. 273–285, 1998.
- [80] F. G. Hall, K. F. Huemmrich, and S. N. Goward, "Use of narrow-band spectra to estimate the fraction of absorbed photosynthetically active radiation," *Remote Sens. Environ.*, vol. 32, no. 1, pp. 47–54, 1990.
- [81] C. D. Elvidge and Z. Chen, "Comparison of broad-band and narrow-band red and near-infrared vegetation indices," *Remote Sens. Environ.*, vol. 54, no. 1, pp. 38–48, 1995.
- [82] A. Savitzky and M. J. Golay, "Smoothing and differentiation of data by simplified least squares procedures," *Anal. Chem.*, vol. 36, no. 8, pp. 1627–1639, 1964.



- [83] P. J. Zarco-Tejada, J. C. Pushnik, S. Dobrowski, and S. L. Ustin, "Steady-state chlorophyll a fluorescence detection from canopy derivative reflectance and double-peak red-edge effects," *Remote Sens. Environ.*, vol. 84, no. 2, pp. 283–294, 2003.
- [84] R. F. Kokaly and R. N. Clark, "Spectroscopic determination of leaf biochemistry using band-depth analysis of absorption features and stepwise multiple linear regression," *Remote Sens. Environ.*, vol. 67, pp. 267–287, 1999.
- [85] S. Wold, M. Sjöström, and L. Eriksson, "PLS-regression: A basic tool of chemometrics," *Chemometr. Intell. Lab. Syst.*, vol. 58, no. 2, pp. 109–130, 2001.
- [86] E. M. Middleton *et al.*, "Linking foliage spectral responses to canopy level ecosystem photosynthetic light use efficiency at a Douglas-fir forest in Canada," *Can. J. Remote Sens.*, vol. 35, no. 2, pp. 166–188, 2009.
- [87] Y.-B. Cheng, E. M. Middleton, T. Hilker, N. C. Coops, T. A. Black, and P. Krishnan, "Dynamics of spectral bio-indicators and their correlations with light use efficiency using directional observations at a Douglas-fir forest," *Meas. Sci. Technol.*, vol. 20, no. 9, pp. 095107–095122, 2009.
- [88] Y.-B. Cheng *et al.*, "Utilizing in situ directional hyperspectral measurements to validate bio-indicator simulations for a corn crop canopy," *Ecolog. Inform.*, vol. 5, pp. 330–338, 2010.
- [89] G. G. Drolet *et al.*, "Regional mapping of gross light-use efficiency using MODIS spectral indices," *Remote Sens. Environ.*, vol. 112, no. 6, pp. 3064–3078, 2008.
- [90] E. M. Middleton, K. F. Huemmrich, D. R. Landis, T. A. Black, A. G. Barr, and J. H. McCaughey, "Photosynthetic efficiency of northern forest ecosystems using a MODIS-derived photochemical reflectance index (PRI)," *Remote Sens. Environ.*, vol. 187, pp. 345–366, 2016.



**Karl Fred Huemmrich** received the B.S. degree in physics from Carnegie-Mellon University, Pittsburgh, PA, USA, and the Ph.D. degree in geography from the University of Maryland College Park, College Park, MD, USA, in 1995.

He is currently a Research Associate Professor with the Joint Center for Earth Systems Technology and is affiliated with the Department of Geography and Environmental Systems, University of Maryland Baltimore County, Baltimore, MD. He is also an Associate Research Scientist with the Biospheric Sciences Laboratory, NASA's Goddard Space Flight Center, Greenbelt, MD.

He has developed and used models of light interactions with vegetation, and has studied the use of remotely sensed data to collect information on biophysical variables and land cover type using both computer models and field measurements. His research has involved fieldwork in a variety of habitats including working on operations and data analysis for the Boreal Ecosystem and Atmosphere Study (BOREAS) and the First International Satellite Land Surface Climatology Project Field Experiment (FIFE). He is an investigator in the Arctic-Boreal Vulnerability Experiment field study.



**Petya K. Entcheva Campbell** received the B.S. degree in forest engineering from the University of Forest Engineering, Sofia, Bulgaria, in 1988; the M.S. degree in forest silviculture and ecology from the University of Massachusetts at Amherst, Amherst, MA, USA, in 1994; and the Ph.D. degree in forest analysis/remote sensing from the University of New Hampshire, Durham, NH, USA, in 2000.

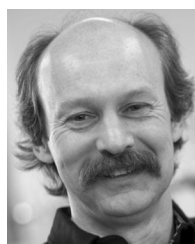
She is currently a Research Associate Professor with the Joint Center for Earth Systems Technology, and is affiliated with the Department of Geography and Environmental Systems (GES), University of Maryland Baltimore County (UMBC), Baltimore, MD, USA; and she is also an Associate Research Scientist with the Biospheric Sciences Laboratory, NASA's Goddard Space Flight Center (GSFC), Greenbelt, MD. Her expertise combines forest ecosystem dynamics and vegetation function assessments, and spectral analyses using satellite (Earth Exploring One (EO-1) Hyperion, HICO), airborne (ASAS, AVIRIS, and MASTER), field, and laboratory spectrometers. At NASA/GSFC, she contributes to the studies of vegetation spectral bioindicators of plant stress, photosynthetic function, and plant fluorescence; and is a member of the Mission Science Team for the Earth EO-1 satellite, and the GSFC group for the NASA HyspIRI satellite concept development. At GES/UMBC, she teaches the remote sensing for environmental applications undergraduate/graduate classes. She coordinates the GOF-C-GOLD South Central and Eastern European Regional Information Network and previously served as the Technical Secretariat for the CEOS Working Group on Calibration and Validation.



**Bo-Cai Gao** received the B.S. degree in physics from Nankai University, Tianjin, China, in 1982, and the M.S. and Ph.D. degrees in physics from Ohio State University, Columbus, OH, USA, in 1984 and 1988, respectively.

He is currently in the Remote Sensing Division, Naval Research Laboratory, Washington, DC, USA. He is a member of the MODIS Science Team, where his focus is on the remote sensing of cirrus clouds, atmospheric water vapor, and coastal water.

Dr. Gao received a Prize Paper Award from the IEEE Geoscience and Remote Sensing Society in 1991 for his development of an operational atmospheric radiative transfer code to retrieve surface reflectance spectra from hyperspectral imaging data measured with the NASA/JPL airborne visible/infrared imaging spectrometer.



**Larry B. Flanagan** received the B.Sc. and M.Sc. degrees from the Department of Botany, University of Alberta, Edmonton, AB, Canada, and the Ph.D. degree from the University of Toronto, Toronto, ON, Canada, in 1988.

He was a NSERC Postdoctoral Fellow with the Lab of Jim Ehleringer, Department of Biology, University of Utah. He was an Assistant and Associate Professor with Carleton University, Ottawa, Canada, during 1991–1997. In 1997, he was an Associate Professor with the University of Lethbridge, Lethbridge, AB, where he is currently a Professor of biology and Board of Governors Research Chair. His previous research interests include ecosystems, including the semiarid grassland of southern Alberta, the boreal forest and peatlands of northern Canada, and the tropical rain forest in the Amazon Basin of Brazil.

His current research interests include applying a range of techniques from plant ecophysiology and ecosystem ecology to understand the acclimation of plants and ecosystems to environmental change. He was an investigator in BOREAS, the Fluxnet-Canada Research Network, the Canadian Carbon Program, Ameriflux, and LBA-Ecology.

**Michael Goulden** received the B.A. degree in biology from Reed College, Portland, OR, USA, and the Ph.D. degree in biological sciences from Stanford University, Stanford, CA, USA, in 1992.

He was a Postdoctoral Fellow with Harvard University in Earth and Planetary Sciences before joining the Department of Earth System Science, University of California, Irvine, CA, in September 1997. His research interests include biological and physical controls on terrestrial nutrient, carbon, and energy cycling, with an emphasis on the response of natural ecosystems to environmental change.